Available online at www.sciencedirect.com

SCIENCE DIRECT®

Biochimica et Biophysica Acta 1666 (2004) 118–141

BIOCHIMICA ET BIOPHYSICA ACTA
BBA

http://www.elsevier.com/locate/bba

Review

The protein–lipid interface: perspectives from magnetic resonance and crystal structures

Derek Marsh[a,*], Tibor Páli[b]

[a]*Max-Planck-Institut für biophysikalische Chemie, Abt. Spektroskopie, 37070 Göttingen, Germany*
[b]*Institute of Biophysics, Biological Research Centre, 6701 Szeged, Hungary*

Received 1 March 2004; received in revised form 13 August 2004; accepted 13 August 2004
Available online 8 September 2004

Abstract

Lipid–protein interactions in membranes are dynamic, and consequently are well studied by magnetic resonance spectroscopy. More recently, lipids associated with integral membrane proteins have been resolved in crystals by X-ray diffraction, mostly at cryogenic temperatures. The conformation and chain ordering of lipids in crystals of integral proteins are reviewed here and are compared and contrasted with results from magnetic resonance and with the crystal structures of phospholipid bilayers. Various aspects of spin-label magnetic resonance studies on lipid interactions with single integral proteins are also reviewed: specificity for phosphatidylcholine, competition with local anaesthetics, oligomer formation of single transmembrane helices, and protein-linked lipid chains. Finally, the interactions between integral proteins and peripheral or lipid-linked proteins, as reflected by the lipid–protein interactions in double reconstitutions, are considered.

Keywords: Spin-label; EPR; Torsion angle; Order parameter; PDC-109; Seminal plasma protein; Acetylcholine receptor; Phospholamban; Avidin; Cytochrome oxidase; Cytochrome *c*; Myelin proteolipid; Myelin basic protein; Biotinyl lipid; Local anaesthetic

Contents

* Corresponding author. Tel.: +49 551 201 1285; fax: +49 551 201 1501.
E-mail address: dmarsh@gwdg.de (D. Marsh).

0005-2736/$ - see front matter © 2004 Elsevier B.V. All rights reserved.
doi:10.1016/j.bbamem.2004.08.006

1. Introduction

Because of the favourable time scale of nitroxide EPR spectroscopy (see e.g., Ref. [1]), spin-labelled lipids at the intramembranous perimeter of integral proteins are resolved spectrally from those in the fluid bilayer regions of the membrane. In this way, the stoichiometry and specificity of lipid interactions with membrane-penetrant proteins may be determined. An association constant for equilibrium lipid exchange at the protein interface:

$$\mathrm{PL} + \mathrm{L}^* \rightleftharpoons \mathrm{PL}^* + \mathrm{L}$$

is defined for each site by:

$$K_i = L^*_{\mathrm{b}_i} L_{\mathrm{f}} / \left(L_{\mathrm{b}_i} L^*_{\mathrm{f}} \right) \tag{1}$$

where L_{b_i} and $L^*_{\mathrm{b}_i}$ are the moles of unlabelled and labelled lipid that are associated at site i, and L_{f} and L^*_{f} are defined similarly for the free (i.e., non-associated) lipid populations. The average relative association constant, $K^{\mathrm{L}}_{\mathrm{r}}$, that is measured by EPR at low label concentrations is given by [2,3]:

$$K^{\mathrm{L}}_{\mathrm{r}} = \sum_{i=1}^{m} n_i K_i / N_{\mathrm{b}} \tag{2}$$

where n_i is the number of association sites of type i and $N_{\mathrm{b}} = \sum_i n_i$ is the total number of lipid association sites at the intramembranous surface of the protein. In a standard EPR experiment, the fraction, f, of spin-labelled lipid L that is motionally restricted at the protein surface is given by [2,3]:

$$f = N_{\mathrm{b}} K^{\mathrm{L}}_{\mathrm{r}} / \left[n_{\mathrm{t}} + N_{\mathrm{b}} \left(K^{\mathrm{L}}_{\mathrm{r}} - 1 \right) \right] \tag{3}$$

where n_{t} is the total lipid/protein mole ratio in the sample, and $K^{\mathrm{L}}_{\mathrm{r}}$ is defined relative to the background unlabelled host lipid of the membrane. The stoichiometry (i.e., N_{b}) and selectivity (i.e., $K^{\mathrm{L}}_{\mathrm{r}}$) of lipid interactions with a wide range of integral membrane proteins have been determined by this method, either in reconstituted systems or in natural membranes that are specifically enriched in a particular transmembrane protein. These results have been reviewed in a previous issue of this journal that was devoted to lipid–protein interactions [4]. This latter review also contains a consideration of the membrane insertion of soluble (but membrane-penetrant) proteins, such as apocytochrome *c* and myelin basic protein.

The dynamic ordering of the lipid chains at the protein interface is studied less readily by spin-label EPR than are the stoichiometry and selectivity of interaction. This is because the dynamics of the protein-associated lipid chains lie in the so-called slow-motional regime (which is the reason that they can be resolved spectrally). In this regime, the lipid chain ordering can be determined only from EPR studies on aligned membranes. This has been done for oriented rod outer segment discs, from which it was concluded that there is a wide orientational distribution, i.e., a considerable degree of disorder, of the lipid chain segments associated with rhodopsin [5]. Information on lipid ordering at the protein interface that is obtained from ^{2}H-NMR of deuterated lipid chain segments is more indirect in the sense that this lipid population is not resolved specifically on the ^{2}H-NMR time scale. All lipid environments are in fast exchange on the much slower NMR time scale, and chain ordering at the lipid–protein interface is reflected by that of the mean order parameter $\langle S_{\mathrm{mol}} \rangle$ for all lipids [6,7]. A general feature found from such measurements is that the orientational order of the lipid chains at the protein interface is not greatly different from that in fluid lipid bilayer membranes [8,9]. This is a necessary requirement for good matching between the hydrophobic span of the protein and that of the fluid lipid chains [10]. However, although the mean order parameter changes relatively little, the spread of chain order parameters increases progressively with the amount of protein in the membrane [11]. This suggests that a more heterogeneous environment exists at the protein–lipid interface than in the bulk fluid regions of the membrane.

Recently, the number of structures of transmembrane proteins that have been obtained by X-ray crystallography has increased considerably. In several cases, this now extends to detection of a number of phospholipids (or glycolipids) that remain associated with the integral proteins in crystals (see Table 1). The first part of this

Table 1
Lipids associated with integral membrane proteins in the protein database

Lipid	Protein	Resolution (nm)	PDB file	Reference
Ste_2PtdCho	*P. denitrificans* CO	0.30	1QLE	[12]
Ste_2PtdEtn	*Rb. sphaeroides* CO	0.23	1M56	[13]
PalLinPtdCho	bovine CO	0.18	1V54	[14]
SteΔ_4AchPtdEtn	bovine CO	0.18	1V54	[14]
PalVacPtdGro	bovine CO	0.18	1V54	[14]
$(Acyl_2Ptd)_2$Gro	bovine CO	0.18	1V54	[14]
$Acyl_2$PtdEtn	*S. cerevisiae* CR	0.23	1KB9	[15]
$Acyl_2$PtdCho	*S. cerevisiae* CR	0.23	1KB9	[15]
$Acyl_2$PtdIns	*S. cerevisiae* CR	0.23	1KB9	[15]
$(Acyl_2Ptd)_2$Gro	*S. cerevisiae* CR	0.23	1KB9	[15]
$Acyl_2$PtdEtn	chicken CR	0.316	1BCC	[16]
$Acyl_2$PtdCho	bovine ADP/ATP	0.22	1OKC	[17]
$(Acyl_2Ptd)_2$Gro	bovine ADP/ATP	0.22	1OKC	[17]
$Acyl_2$PtdCho	*Rb. sphaeroides* RC	0.255	1M3X	[18]
(Glc Gal) $acyl_2$Gro	*Rb. sphaeroides* RC	0.255	1M3X	[18]
$(Acyl_2Ptd)_2$Gro	*Rb. sphaeroides* RC	0.255	1M3X	[18]
$(Acyl_2Ptd)_2$Gro	*Rb. sphaeroides* RC	0.21	1QOV	[19]
$(Acyl_2Ptd)_2$Gro	*Rb. sphaeroides* RC	0.27	1E14	[20]
Pam_2PtdEtn	*Tch. tepidum* RC	0.22	1EYS	[21]
Pam_2PtdGro	*S. elongatus* PS I	0.25	1JB0	[22]
Galactosyl Ste_2Gro	*S. elongatus* PS I	0.25	1JB0	[22]
Ole_2PtdCho	*M. laminosus* cyt b_6f	0.30	1UM3	[23]
$(Acyl_2Ptd)_2$Gro	*E. coli* Fdh-N	0.16	1KQF	[24]
$(Acyl_2Ptd)_2$Gro	*E. coli* Sdh	0.26	1NEK	[25]
$Acyl_2$PtdEtn	*E. coli* Sdh	0.26	1NEK	[25]
$Acyl_2$Gro	*S. lividans* KcsA	0.20	1K4C	[26]
Phy_2Gro	*H. salinarum* bR	0.27	1BRR	[27]
Triglycosyl Phy_2Gro	*H. salinarum* bR	0.27	1BRR	[27]
Phy_2Gro	*H. salinarum* bR	0.155	1C3W	[28]
Phy_2Gro	*H. salinarum* bR	0.19	1QHJ	[29]
Phy_2Ptd	*H. salinarum* bR	0.25	1QM8	[30]
(Triglycosyl) Phy_2Gro	*H. salinarum* bR	0.25	1QM8	[30]
Phy_2PtdGro*P*	*H. salinarum* bR	0.25	1QM8	[30]
Phy_2PtdGro	*H. salinarum* bR	0.25	1QM8	[30]
LPS	*E. coli* FhuA	0.25	1QFG	[31]

Abbreviations: Ptd, phosphatidyl; Cho, choline; Gro, glycerol; Etn, ethanolamine; Ins, inositol; Glc, glucose; Gal, galactose; Ste, stearoyl; Pam, palmitoyl; Phy, phytanyl; Lin, linoleoyl; Vac, vaccenoyl; Δ_4Ach, arachidonoyl; LPS, lipopolysaccharide; CO, cytochrome *c* oxidase; CR, cytochrome *c* reductase (cytochrome bc_1 complex); ADP/ATP, ADP/ATP carrier; RC, photosynthetic reaction centre; PS, photosystem; cyt. b_6f, cytochrome b_6f complex; Fdh-N, nitrate-induced formate reductase; Sdh, succinate dehydrogenase; KcsA, pH-gated potassium channel; bR, bacteriorhodopsin; FhuA, Fe-siderophore active transporter.

review is devoted to describing and contrasting those features of membrane proteins in crystals that are relevant to the abovementioned magnetic resonance studies of lipid–protein interactions in fully hydrated lipid membranes at near-physiological temperatures. The stoichiometry of lipid association at the intramembranous perimeter of the protein is investigated by model building. The molecular configurations of the lipid molecules in protein crystals are analysed in terms of those in single crystals of phospholipids and of the dynamic configurations in fluid phospholipid bilayers. Finally, the static distributions of lipid chain order parameters that are calculated from the crystal structures are compared with the dynamic lipid chain order parameters determined by magnetic resonance.

The second part of this review is devoted to further spin-label EPR results on lipid–protein interactions that were not included in the previous review of this series [4]. Various aspects of lipid interactions with single proteins are dealt with: specificity for phosphatidylcholine, competition with local anaesthetics, oligomer formation of bitopic proteins, and protein-linked lipids. This is then followed by examples of the interaction of membrane-spanning proteins with peripheral and lipid-anchored proteins that are investigated via the lipid–protein interactions in double-reconstituted systems.

2. Stoichiometry of lipid interactions with integral proteins

Lipid–protein titrations with reconstituted membranes have established that the number of motionally restricted lipids per protein, N_b, is independent of the total lipid/protein ratio, n_t [2,32–40]. In this sense, the motionally restricted lipids can be defined operationally as a first shell surrounding the protein. It is therefore expected that this fixed lipid stoichiometry is related directly to the transmembrane

structure, and degree of oligomerisation, of the protein. From simple geometric considerations for helical sandwiches or regular polygons of moderate size, it is predicted that the number of perimeter lipids depends linearly on the number, n_α, of transmembrane α-helices per monomer [41]:

$$N_b = \pi(D_\alpha/d_{ch} + 1) + n_\alpha D_\alpha/d_{ch} \quad (4)$$

where D_α and d_{ch} are the diameters of an α-helix and a lipid chain, respectively, ($D_\alpha/d_{ch} \approx 2.1$), and $n_\alpha > 1$. For a single transmembrane helix, $N_b \approx 10$–12. Eq. (4) also applies to protein oligomers, if the monomers are roughly circular in cross-section and are packed in a manner similar to that assumed above for α-helices. Then D is the diameter of the protein monomer and n is the aggregation number. If, on the other hand, the oligomer packing is tighter and preserves the helical sandwich motif throughout the oligomer (i.e., the individual helices, rather than the whole proteins, are packed according to Eq. (4)), the number of perimeter lipids per monomer is given from Eq. (4) by:

$$N_b^{(1)} = (\pi/n_{agg})(D_\alpha/d_{ch} + 1) + n_\alpha D_\alpha/d_{ch} \quad (5)$$

where n_{agg} is the number of monomers per oligomer. This simple model approximates reasonably well the lipid stoichiometries that are determined by spin-label EPR for small proteins, but overestimates the stoichiometry of the motionally restricted lipids for larger proteins [41].

A more detailed estimate of the number of first-shell lipids can be obtained from the crystal structures of integral membrane proteins by using molecular modelling [42]. Fig. 1 shows the structure of bovine rhodopsin (Ref. [43]; PDB 1L9H), together with space-filling models of dimyristoyl phosphatidylcholine (myr_2PtdCho). The lipid chains are shortened from their all-*trans* length (by using a tether function—Ref. [44]) and positioned vertically around the protein to achieve good hydrophobic matching. They are close-packed around the protein by applying external inward-directed forces to each lipid atom. The structure is energy-minimised by using the MM3 force field [45].

Previously, the above procedure was applied successfully to lipidation of the M13 phage coat protein, when analysing results from site-directed spin-labelling of the protein [46]. Twelve dioleoyl phosphatidylcholine molecules can be accommodated around the single transmembrane helix of this bitopic protein. This latter value agrees well with the number of motionally restricted lipids associated with the L37A mutant of phospholamban, for which mutation of the leucine zipper in the single transmembrane helix prevents oligomer formation [40]. The wild-type M13 coat protein itself forms oligomers in dioleoyl phosphatidylcholine bilayers [38].

The number of dimyristoyl phosphatidylcholine lipids that can be accommodated around the intramembranous perimeter of the rhodopsin structure in Fig. 1 is ca. 27±2. For comparison, the number of lipids motionally restricted by bovine rhodopsin reconstituted in dimyristoyl phosphatidylcholine bilayers is 22±2 [36]. Corresponding values in native membranes are: 25±3 and 23±2 lipids per rhodopsin for bovine and frog rod outer segment discs, respectively [47,48]. The prediction from Eq. (4) is N_b=24 for a seven-helix sandwich. Thus all estimates agree reasonably well, in this case. The motionally restricted lipid population that is detected by spin-label EPR approximately is sufficient to constitute a complete shell of lipids surrounding the intramembranous perimeter of rhodopsin. Also, Eq. (4) gives a reasonable approximation for helical sandwiches such as rhodopsin (i.e., for n_α~7), even when the helices are tilted somewhat.

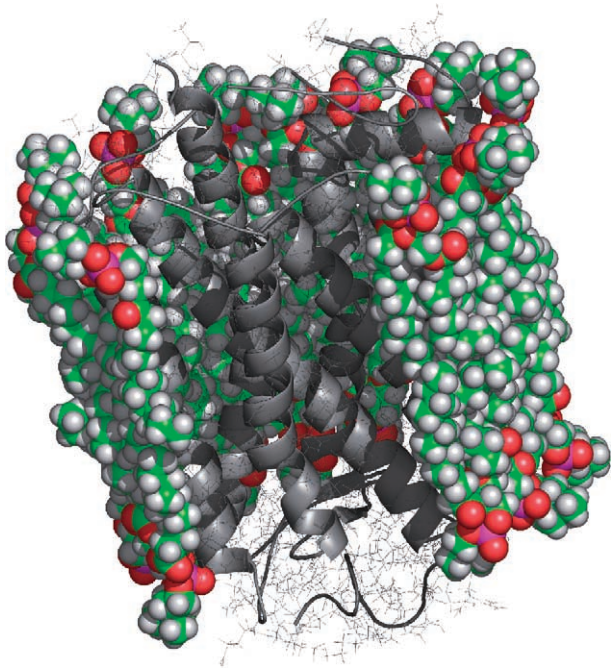

Fig. 1. Crystal structure of bovine rhodopsin (Ref. [43]; PDB:1L9H), in ribbon and wire-frame representation, surrounded by a single bilayer shell of energy-minimised myr_2PtdCho lipids (see text). For clarity, only part of the lipid shell is shown—in space-filling representation [42].

Fig. 2 compares the stoichiometries of motionally restricted lipids associated with various proteins that are determined by spin-label EPR with the numbers of first-shell lipids that are obtained by molecular modelling. The geometric predictions of Eqs. (4) and (5) for monomers and hexamers also are shown, by the solid and dotted lines, respectively. The number of first-shell lipids that can be accommodated around bacteriorhodopsin (N_b=24–25) is slightly smaller than for rhodopsin because the helices of the seven-helix bundle are tilted less in bacteriorhodopsin than in the G protein-coupled visual receptor. Both are in approximate accord with spin-label EPR experiments and estimates from Eq. (4). For both the SERCA Ca^{2+}-ATPase and the nicotinic acetylcholine receptor (nAcChoR), the number of lipids motionally restricted is less than the number of first-shell lipids that is obtained by molecular modelling. In the former case,

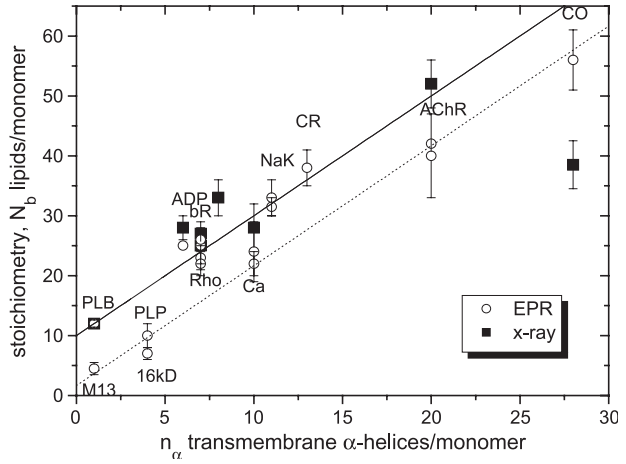

Fig. 2. Number, N_b, of first-shell lipids interacting with different integral proteins composed of n_α transmembrane helices per monomer. Solid squares correspond to the first shell of lipids surrounding the X-ray structure of the protein, as determined by model building [42]. Open circles correspond to the motionally restricted lipids that are resolved by EPR spectroscopy (see Ref. [41], for references). Solid line: prediction of Eq. (4) for helical sandwiches or regular polygons. Dotted line: prediction of Eq. (5) for hexamers (n_{agg}=6). M13, M13 bacteriophage coat protein; PLB, L37A mutant of phospholamban; PLP, myelin proteolipid protein; 16 kD, 16-kDa proteolipid from *Nephrops*; ADP, ADP-ATP carrier; Rho, rhodopsin; Ca, Ca-ATPase; NaK, Na,K-ATPase; CR, cytochrome reductase; AChR, acetylcholine receptor; CO, cytochrome oxidase. Labels are positioned horizontally to correspond to the appropriate values of n_α.

the number of first-shell lipids lies between the stoichiometries of the Ca^{2+}-ATPase and the Na^+,K^+-ATPase, both of which are P-type ATPases and are thought to have the same number of transmembrane helices, apart from the extra single transmembrane domain contributed by the β-subunit of the Na,K-ATPase.

The nAcChoR has an extremely angular, star-shaped cross-section [49]. Possibly the intramembranous surface at the apices of the star, which correspond to a single transmembrane helix from each subunit, is insufficient to restrict lipid-chain motion appreciably (see Section 4.3 later, for discussion of single transmembrane helices). The motionally restricted lipids detected by spin-label EPR spectroscopy may constitute only those perimeter lipids that are located in the invaginated regions, along the arms of the star. Spin-label studies with the acetylcholine receptor are described later in Section 4.2.

In conclusion, it should be emphasised that the strategy adopted in the molecular modelling is directed solely at determining the lipid stoichiometry. The aim is to ensure complete filling of volume at the lipid–protein interface, for good hydrophobic matching irrespective of chain configuration. In reality, there may be a mixing of chains between first and second shells, but this does not alter the net stoichiometry of chain segments directly contacting the protein. The molecular modelling is not intended to reproduce the exact chain configurations of the protein-interacting first-shell lipids. This latter topic is dealt with in the forthcoming sections.

3. Crystals of integral membrane proteins

Several crystal structures of transmembrane proteins in the Protein Data Base now contain one or more associated phospho- or glycolipids (see Fig. 3 and Table 1). In most cases, the number of lipids resolved crystallographically is far from sufficient for complete coverage of the intramembranous protein surface. A near-exception is the nine distinct diphytanyl lipids resolved in association with bacteriorhodopsin trimers [29]. It is therefore appropriate to ask whether the lipids that are identified in crystals of membrane proteins correspond to special, i.e., specific, lipid–protein associations. Or are they generally representative of the lipids that surround proteins in fully hydrated fluid membranes, such as those studied by magnetic resonance spectroscopy?

In the following sections, we review the configuration and molecular ordering of the phospholipids and glycolipids that are resolved crystallographically in association with integral membrane proteins. Polar headgroup and glycerol backbone configurations are compared with those in single crystals of synthetic phospholipids and glycolipids (reviewed in Ref. [51]). The configurational and molecular ordering of the lipid chains is compared with results from magnetic resonance studies.

For comparison with the results on membrane proteins, conformational analysis of phospholipid ligands bound to soluble proteins can be found in Ref. [52]. The definition of the lipid torsion angles that are used for the conformational analysis is given in Fig. 4. The different rotamers are specified by the following torsion angles: antiperiplanar (ap) or *trans* (*t*), 180°; synclinal (±sc) or *gauche* ($g^\pm$), ±60°; anticlinical (±ac) or *skew* ($s^\pm$), ±120°; and synplanar (sp) or *cis* (*c*), 0°. Rotamer populations are described by ±30° ranges about these values.

3.1. Headgroup conformation

In bilayer crystals whose molecular structures have been determined, the phospholipid headgroup is, without exception, oriented preferentially parallel to the bilayer plane and its conformation is rather constant (see Ref. [51]). For phosphatidylethanolamine, its *N*-methyl substituents and phosphatidylcholine, the headgroup conformation in bilayer crystals has the following sequence of torsion angles: α_1=ap, α_2=±sc, α_3=±sc, α_4=ap to ±ac and α_5=∓sc, where the upper and lower combinations of signs are mirror images. In bilayer crystals of phosphatidylglycerol, the two optical enantiomers of the glycerol headgroup have the configuration: α_1=∓ac, α_2=∓sc, α_3=∓sc, α_4=±ac, α_5=ap [53]. The upper sign corresponds to the *sn*-1 enantiomer that is found naturally in eucaryotes and eubacteria, and the lower sign to the *sn*-3 enantiomer found in the archaea.

Table 2 gives the distribution of the polar headgroup torsion angles for the lipids that are associated with integral proteins in the PDB. The upper row of percentage values gives the populations of the rotamers that constitute the

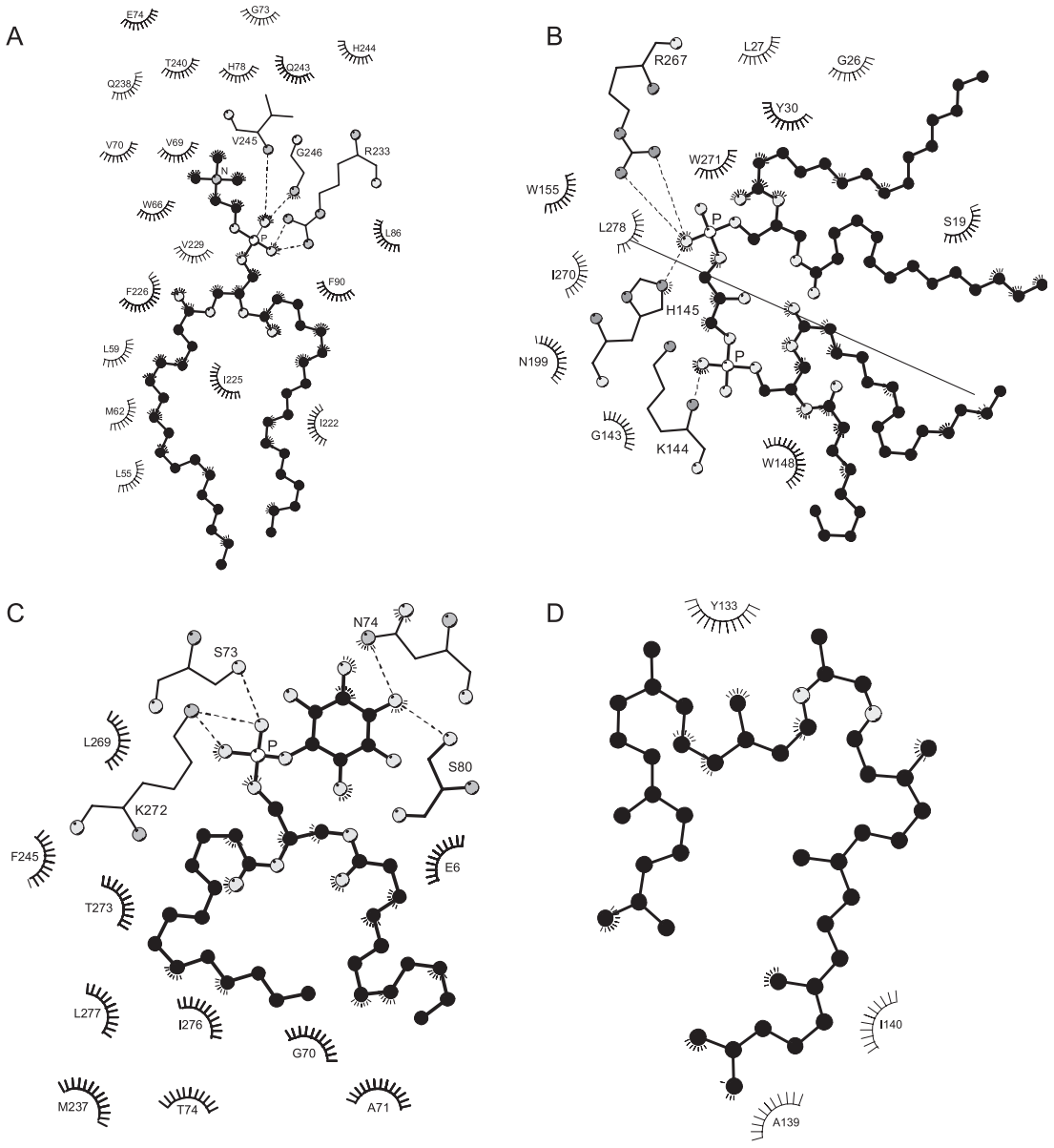

Fig. 3. LIGPLOT diagrams [50] of phospholipids associated with various transmembrane proteins. Neighbouring protein residues that are involved in hydrophobic contacts are indicated, and hydrogen bonds are shown explicitly. C-atoms of the phospholipid are shown as black balls. O-atoms are given in light grey, N-atoms in dark-grey, and P-atoms are white. (A) Phosphatidylcholine in association with *Paracoccus denitrificans* cytochrome *c* oxidase (PDB:1QLE; Ref. [12]). (B) Cardiolipin (diphosphatidylglycerol) in association with *Rb. sphaeroides* photosynthetic reaction centre mutant AM260W (PDB:1QOV; Ref. [19]). (C) Phosphatidylinositol in association with yeast cytochrome *c* reductase (PDB:1KB9; Ref. [15]). (D) Diphytanylglycerol in association with *Halobacterium salinarum* bacteriorhodopsin (PDB:1QHJ); Ref. [29]).

preferred conformation for zwitterionic headgroups in bilayer crystals. The second row of percentage values gives the populations that correspond to the preferred α_1, α_4 and α_5 rotamers in phosphatidylglycerol, and to the rotamer of the energetically second most favourable conformation of the phosphate diester (viz., $\alpha_2/\alpha_3=\pm$sc/ap). Of the 50 complete lipid headgroups from the PDB, only one headgroup moiety of cardiolipin associated with the bacterial reaction centre corresponds fully to the conformation found in single crystals of phospholipids. This and eight other lipids have the energetically most favourable $\pm$sc/$\pm$sc phosphate diester configuration. A further 10 lipids have the next most favourable $\alpha_2/\alpha_3=\pm$sc/ap configuration. Seventeen headgroup moieties have an energetically disfavoured eclipsed conformation for the α_5 C–C torsion angle.

At the protein interface, the spread of polar headgroup orientations and conformations is therefore much wider than in lamellar crystals of diacyl phospholipids [51,55], or in fluid phospholipid bilayers [56,57]. In nearly all cases, the lipid phosphate is anchored by hydrogen bonding to protein residues (see e.g., Fig. 3A,B,C). Other specific interactions with the protein also stabilise headgroup conformations that are not found in bilayer crystals. A similar situation is found with the polar headgroups of phospholipid ligands in the

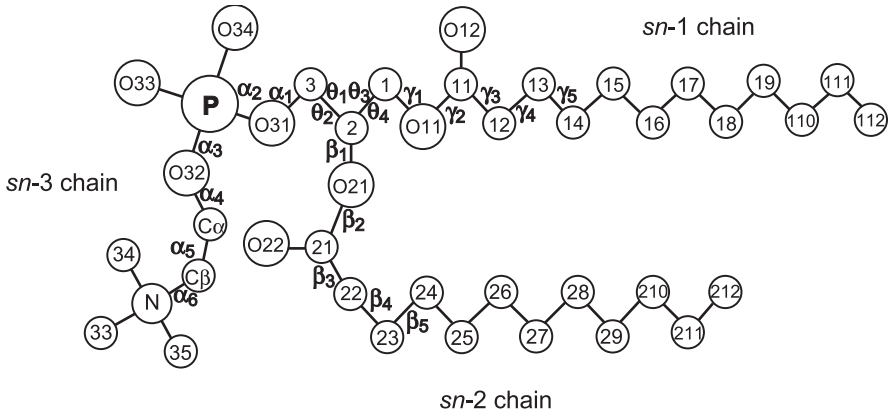

Fig. 4. Designation of phospholipid torsion angles for the headgroup (α_j), glycerol backbone (θ_j), *sn*-1 chain (γ_n), and *sn*-2 chain (β_n). For the glycerol backbone: θ_1≡C(1)–C(2)–C(3)–O(31), θ_2≡O(21)–C(2)–C(3)–O(31), and θ_3≡O(11)–C(1)–C(2)–C(3), θ_4≡O(11)–C(1)–C(2)–O(21) (see also Ref. [51]).

binding pockets of soluble proteins [52]. Specific examples of lipid headgroup interactions with integral membrane proteins are discussed in Ref. [54].

3.2. Glycerol backbone configuration

Glycerolipids of eucaryotes and eubacteria have the *sn*-3 enantiomeric configuration of the glycerol backbone, with the chains attached at the *sn*-1 and *sn*-2 positions. Archaebacterial lipids have the *sn*-1 glycerol configuration, with the chains attached at the *sn*-3 and *sn*-2 positions. The enantiomeric configuration can be deduced from the θ-torsion angles: $\theta_1-\theta_2=\mp120^\circ$ and $\theta_3-\theta_4=\pm120^\circ$, with the upper signs for the *sn*-3 enantiomer and the lower signs for the *sn*-1 enantiomer, and assuming tetrahedral bond angles (see e.g., Ref. [54]). With the exception of the two phosphatidylethanolamines associated with chicken cytochrome *c* reductase and diglycosyl glycerol associated with the bacterial reaction centre, all eucaryotic/eubacterial lipids in Table 1 are the correct glycerol enantiomer. For the archaeal lipids associated with bacteriorhodopsin, however, 5 glycerol structures out of 21 in the PDB are the incorrect enantiomer [54].

Table 2
Distribution of polar headgroup conformations for lipids in membrane protein crystals[a]

α_1	α_2	α_3	α_4	α_5
ap	±sc	±sc	ap	∓sc
61%	51%	39%	38%	32%
∓ac	ap	ap	±ac	ap
33%	14%	26%	44%	34%
Remainder				
6%	35%	35%	18%	34%

[a] The first two rows of percentage values give the population of lipids in protein crystals that have the bilayer-preferred headgroup torsional conformations, α_i, which are indicated in the row immediately above (see text). The final row of percentage values gives the population of lipids in protein crystals that have none of the above values of α_i which are preferred in bilayer crystals. Each α_i column sums to 100%. Total number of lipids=50–54 (see Ref. [54]).

For lipids with the *sn*-3 phosphatidyl/glycosyl configuration, the torsion angles θ_4 and θ_2 specify the relative orientations of the *sn*-1 and *sn*-2 chains, and the orientation of the headgroup relative to the *sn*-2 chain, respectively [51]. *Gauche* (±sc) rotamers for θ_4 allow parallel chain stacking, as in bilayer membranes, and they are favoured energetically for both θ_4 and θ_2 [58]. Table 3 gives the distribution of glycerol backbone configurations for lipids in integral protein crystals, according to the θ_4/θ_2 combination of torsion angles. All those configurations of nonarchaeal lipids with staggered rotamers and parallel-chain orientation are found also represented in bilayer crystals of phospholipids. The relative occurrence in the latter is: 36% sc/sc, 18% −sc/−sc, 6% sc/ap, 9% −sc/ap and 30% sc/−sc [51]. Comparison with Table 3 shows that the protein-interacting lipids are relatively enriched in conformations with θ_2=ap. Protein–lipid interactions must outweigh the intramolecular "gauche effect" that favours θ_2=±sc rotamers, in these cases.

Table 3
Distribution of glycerol backbone configurations for lipids in membrane protein crystals

θ_4/θ_2	θ_3/θ_1	N[a]	Percentage
Staggered, parallel-chain (40%)			
sc/sc	tg^-	10	33
−sc/−sc	g^+t	3	10
	tg^+	1[b]	-
sc/ap	tg^+	9	30
−sc/ap	g^+g^+	2	7
sc/−sc	tt	4	13
−sc/sc	g^+g^-	2	7
	tt	4[b]	-
Staggered, nonparallel-chain (8%)			
ap/−sc	g^-t	2	40
	g^+g^+	2[b]	-
ap/sc	g^-g^-	3	60
Eclipsed (52%)			
		46	

[a] Number of lipid structures. Not all have θ_3/θ_1 values compatible with θ_4/θ_2 (see Ref. [54]).
[b] Archaeal lipids.

Glycerol configurations ap/±sc that do not allow the parallel chain stacking, which is required in bilayer crystals, are also found for some lipids associated with transmembrane proteins. These, and other similar configurations, are found also for phospholipids in the binding sites of soluble proteins [52]. However, 52% of the configurations of the glycerol backbones of lipids associated with integral membrane proteins have one, or both, θ_4/θ_2 rotamers in an eclipsed conformation. These configurations are energetically disallowed for isolated C–C single bonds (see e.g., Ref. [59]).

3.3. Carboxyl ester conformation

Resonance hybridisation of the sp^2 carbon dictates that the ester carboxyl groups of lipid chains should be planar, and *trans* (ap) [55]. Out of a total of 114 γ_2 and β_2 torsion angles for the nonarchaeal lipids in Table 1, 57% have the *trans* (ap) conformation. Of the remainder, 30% are ac, 6% are sc and 7% are *cis* (sp) conformers [54]. The carboxyl torsion angle violations must be attributed presumably either to conformational disorder or to improper optimisation (cf. Ref. [60]). Archaeal lipids have phytanyl chains that are ether-linked and therefore the γ_2 and β_2 torsion angles are less restricted than for ester-linked chains. For the lipids associated with bacteriorhodopsin (see Table 1), the 42 γ_2 and β_2 torsion angles distribute almost equally between the *trans* (33%), *skew* (33%) and *gauche* (29%) conformers (together with 5% *cis*) [54].

3.4. Lipid chain configuration

The lowest-energy conformation for the C–C bonds in lipid alkyl chains is the *trans* (ap) conformer. The other energetically allowed rotamers are the two *gauche*$^{\pm}$ (±sc) conformers (see e.g., Ref. [61]). Eclipsed conformers are, as already mentioned, energetically disallowed.

Fig. 5 shows the torsion angles γ_n and β_n in the *sn*-1 and *sn*-2 chains of the 12 phosphatidylethanolamine molecules associated with the two molecules in the unit cell of *Rhodobacter sphaeroides* cytochrome *c* oxidase [13]. Torsion angles γ_n, β_n with $n \geqslant 3$ correspond to the C–C bonds in the lipid chain. The chains are predominantly in the *trans* (ap) configuration. Relatively few *gauche* (±sc) rotamers are present. However, there is a rather large population of energetically disallowed *skew* (±ac) conformations. Some *cis* conformers are found, exclusively in the *sn*-1 chain, although *cis* double bonds are normally confined to the *sn*-2 chain in naturally occurring lipids.

Fig. 6 gives the distribution of chain torsion angles for all the lipids listed in Table 1. The torsion-angle distribution obtained from a molecular dynamics simulation of fluid phospholipid bilayers is included for comparison. *Trans* (ap) configurations predominate for the protein-associated lipid chains. Chain disorder, however, is mostly associated with *skew* (±ac) conformers, rather than with the energetically allowed *gauche* (±sc)

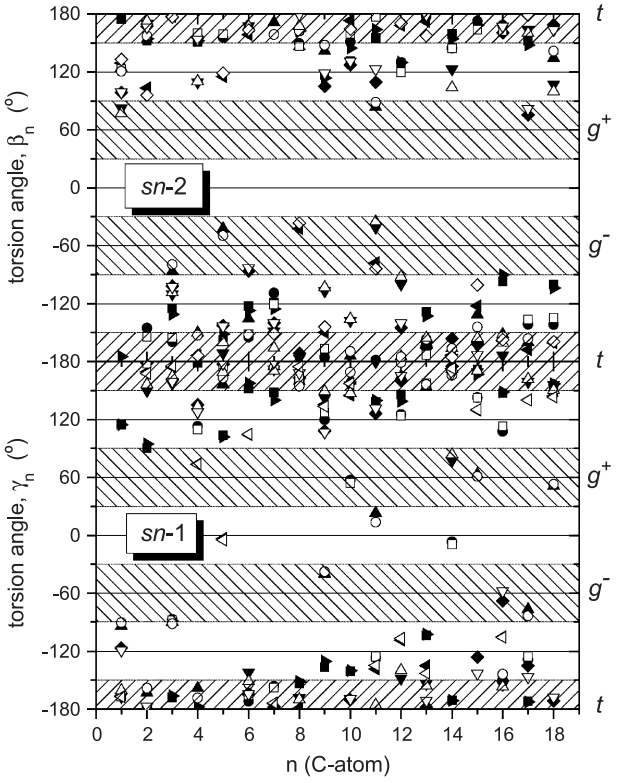

Fig. 5. Torsion angles, $C_{n-3}C_{n-2}C_{n-1}C_n$, in the *sn*-1 (γ_n, lower panel) and *sn*-2 (β_n, upper panel) chains of ste$_2$PtdEtn in crystals of *Rb. sphaeroides* cytochrome *c* oxidase (PDB:1M56; Ref. [13]). Different symbols correspond to the 12 molecules of ste$_2$PtdEtn. Dihedral angles are given as a function of position, C_n, in the chain. The allowed *trans* (*t*) and *gauche*$^{\pm}$ ($g^{\pm}$) conformers are indicated by shading [62].

rotamers. This suggests that torsion angles apparently in the ±(120±30°) ranges may, in fact, represent conformational heterogeneity of the lipid chains in protein crystals. A bias towards *skew* chain conformers, at the expense of *gauche* rotamers, is found also in crystal structures of phospholipid ligands bound to soluble proteins [52]. In part, such discrepancies might also arise from use of inadequate restraint libraries with which to refine the crystallographic structure [60]. On the other hand, the force fields used in the molecular dynamics simulation that is illustrated in Fig. 6 ensure that only staggered conformers appear in the lipid chains. Of relevance for the lipids associated with integral membrane proteins is the fact that the B-values (or "temperature factors"—that are a measure of disorder in the crystal) of lipids in membrane protein crystals are appreciably higher than those for the protein [54]. This is consistent with a distribution of conformations, rather than a single, unique lipid conformer.

3.5. Phytanyl chain configurations

The ether-linked phytanyl chains in archaebacterial lipids contain branched methyl groups in the *R*-configuration at the 3, 7, 11 and 15 positions [64]. Of the 108 chiral centres

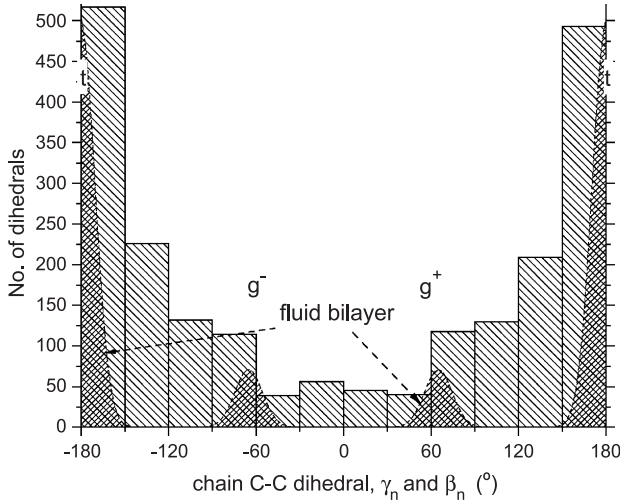

Fig. 6. Histogram: distribution of C–C torsion angles, γ_n and β_n, in the hydrocarbon chains of phospho-/glycolipids in crystals of integral membrane proteins. Dihedral angles are determined for the C_2–C_3 bond onwards, and for all chains with the exception of single-chain fragments. Bin size corresponds to a ±30° range about each staggered (ap, ±sc) or eclipsed (sp, ±ac) rotamer [54]. Dashed lines: distribution of chain torsion angles in fluid lipid bilayer membranes of myr$_2$PtdCho from molecular dynamics simulations [63].

in the chains of diphytanyl lipids interacting with bacteriorhodopsin that appear in Table 1, 31% have the *R*-configuration and 69% have the incorrect *S*-configuration [54]. Only the diphytanyl chains in PDB file 1QM8 [30] have the wholly the correct *R*-configuration.

The presence of branched methyl groups decreases the stability of *trans* (ap), relative to *gauche* (±sc), for the conformation of the adjacent C–C bonds (see e.g., Ref. [59]). The diphytanyl chains of the lipids in PDB file 1BRR [27] have a high proportion of *gauche* rotamers (35% ±sc), and the proportion of *skew* (±ac) conformers is relatively low [54]. However, not all *gauche* rotamers are associated with the methyl-substituted C-atoms. Steric interactions of the branched methyl groups with the protein therefore may also serve to increase the population of *gauche* rotamers. For the remainder of diphytanyl lipid structures associated with bacteriorhodopsin, the population of disallowed, *skew* eclipsed conformers is considerably higher, in line with the general trend for lipid structures in the Protein Database (cf. Fig. 6).

3.6. Lipid chain order parameters

The orientation of a lipid chain segment, relative to the membrane normal, is determined by the orientation, θ_Z, of the chain long-axis, Z, and by the orientation of the chain segment z' -axis relative to the long axis. The long-axis ordering is specified by an order parameter, which is a second-order Legendre polynomial in $\cos\theta_Z$:

$$S_{ZZ} = \frac{1}{2}\langle 3\cos^2\theta_Z - 1\rangle \qquad (6)$$

where the angular brackets denote an ensemble or time average. The local segmental ordering, $S_{z'z'}$, is determined by the limited number of distinct orientations that are allowed by the tetrahedral geometry of an sp^3 C–C bond. The latter are specified by the local torsion angle (t, g^+) together with the angle (0°, 60° or 90°) that the segment axis makes with the initial *trans* segments (see e.g., Ref. [61]). Table 4 gives the chain order parameters and local conformational populations that are obtained for three deuteration positions of the *sn*-2 chain of dimyristoyl phosphatidylcholine in fluid bilayer membranes [65]. The values of the chain long axis order parameter S_{ZZ} are comparable to that which can be estimated for the C(1)–C(3) axis of the glycerol backbone: $S_{C1-C3} \approx 0.44$ in dipalmitoyl phosphatidylcholine bilayers at 49 °C (see Ref. [66]). From the addition theorem for Legendre polynomials, the net segmental order parameter at chain position i is given by: $S_{mol,i}=S_{ZZ}\times S_{z'z',i}$. These values are also listed in Table 4.

Comparison of the segmental ordering of the lipid chains in protein crystals with the results from magnetic resonance requires averaging over the chain sites on the protein. The order parameter of segment C_i is then given by:

$$S_{mol,i} = \frac{3}{2N_{ch}}\sum_{m=1}^{N_{ch}}\cos^2\theta_{i,m} - \frac{1}{2} \qquad (7)$$

where $\theta_{i,m}$ is the tilt to the membrane normal of the C_{i-1}–C_{i+1} vector in chain m, and N_{ch} is the number of chains averaged over. Fig. 7 gives the order parameter profiles of the diphytanyl chains associated with bacteriorhodopsin and of the phospholipid acyl chains associated with *S. cerevisiae* cytochrome *c* reductase. For comparison, the chain order profiles at two different temperatures in fluid dipalmitoyl phosphatidylcholine bilayers are also included in Fig. 7. The order of the protein-associated lipids differs considerably between the two hydrocarbon chains, which is not the case along most of the length of the *sn*-1 and *sn*-2 chains in fluid phospholipid bilayer membranes [67]. Further, the order profiles averaged over the two chains differ markedly from those for fluid phosphatidylcholine membranes. The chain

Table 4
Lipid ordering and conformation in the *sn*-2 chain of dimyristoyl phosphatidylcholine membranes in the fluid phase (T=40 °C) [65]

Chain segment	Order parameters[a]			Conformational population[b]		
	S_{ZZ}	$S_{z'z'}$	S_{mol}	$p(t,0°)$	$p(g^{\pm},60°)$	$p(g^{\pm},90°)$
C-6	0.50	0.74	0.37	0.80	0.20	0.00
C-10	0.50	0.56	0.28	0.66	0.28	0.06
C-13	0.50	0.35	0.18	0.51	0.36	0.13

[a] S_{ZZ} is the principal order parameter of the chain long axis; $S_{z'z'}$ is the principal order parameter of the chain segment. The net order parameter is $S_{mol}=S_{ZZ}S_{z'z'}$.

[b] Chain configurations are characterised by the conformation (*trans*, *gauche*$^{\pm}$) relative to the previous segment, and by the orientation (0°, 60°, 90°, 120° or 180°) of the segment axis relative to the initial *trans* segments (see e.g., Ref. [61]).

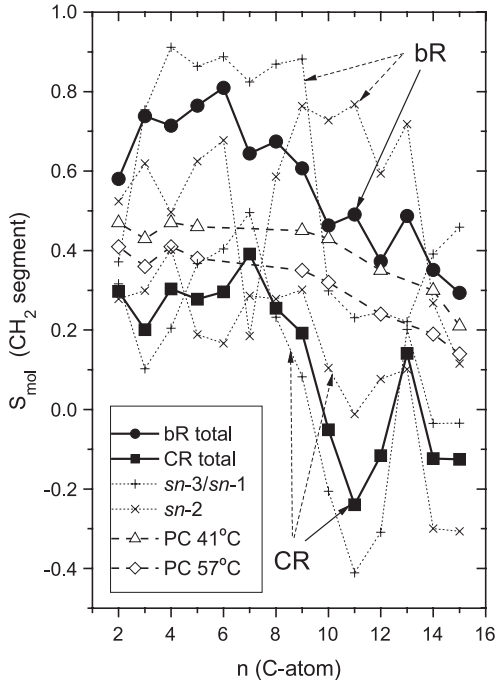

Fig. 7. Segmental order parameter, S_{mol}, as a function of chain position, i=n, for diphytanyl glycerol moieties in association with *H. salinarum* bacteriorhodopsin (bR) (Ref. [28]; PDB:1C3W) and for phospholipids associated with *S. cerevisiae* cytochrome *c* reductase (CR) (Ref. [15]; PDB:1KB9). Mean values of all bR phytanyl chains (-●-) and all CR acyl chains (-■-); mean values of assigned *sn*-2 chains (×), and of bR *sn*-3 or CR *sn*-1 chains (+). Data from Ref. [54]. Experimental values for the mean of the *sn*-1 and *sn*-2 chains in fluid dipalmitoyl phosphatidylcholine bilayers at 41 °C (···△···) and 57 °C (···◇···) are deduced from ^{2}H-NMR order parameters (S_{CD}) by assuming axial symmetry [67].

order for cytochrome *c* reductase lipids is lower, and that for bacteriorhodopsin lipids is consistently higher than the fluid bilayer reference.

Table 5 gives the mean segmental order parameters that are averaged over the length of the lipid chain:

$$\langle S_{mol}\rangle = \frac{1}{n_c - 1}\sum_{i=2}^{n_c} S_{mol,i} \qquad (8)$$

where n_c-1 is the number of chain segments, i, that are summed over. Also listed in Table 5 are the root-mean-square widths of the distribution of segmental order parameters, $\langle(S_{mol,i}-\langle S_{mol}\rangle)^2\rangle^{1/2}$, about the average over the entire chain. For comparison, the mean order parameter in fluid dipalmitoyl phosphatidylcholine bilayers is $\langle S_{mol}\rangle$=0.40–0.31 over the temperature range 41–50 °C, with a distribution width $\langle(S_{mol,i}-\langle S_{mol}\rangle)^2\rangle^{1/2}$ =0.08 that is practically constant. Although the data given in Table 5 correspond to those protein crystals with the largest number of lipids associated (see Ref. [54]), the spread in values of the mean order parameter is wide and the distribution widths are consistently very high, compared with fluid bilayers.

The order parameter distribution widths deduced from ^{2}H-NMR measurements in protein-containing membranes are also larger than those in protein-free lipid bilayers. Fig. 8 gives the mean lipid segmental order parameters and their distribution widths for the visual receptor rhodopsin that is reconstituted in fluid dimyristoyl phosphatidylcholine bilayers at different protein/lipid ratios. The distribution width, but not the mean lipid chain order parameter, increases systematically with increasing protein content. The approximately linear dependence on protein/lipid ratio (as expected for fast exchange) extrapolates to a limiting value of $\langle(S_{mol}-\langle S_{mol}\rangle)^2\rangle^{1/2}$=0.28, at a stoichiometry of ca. 22 lipids/rhodopsin that is consistent with spin-label EPR measurements [36]. Comparison with Table 5 reveals that the spread of disorder of the lipid chains which are resolved in integral membrane protein crystals is greater than that of the full population of lipids at the intramembranous perimeter of the protein. The crystallographically resolved lipid chains are adapted more intimately to the protein surface, and consequently the mean order parameters do not fulfil so well the energetic requirements for hydrophobic matching with the fluid bilayer lipids.

3.7. Conclusions from protein crystals

Conformational violations of the type described in Sections 3.1–3.4 also are not atypical for the structures of lipid ligands in crystals of soluble proteins [52]. Conformational heterogeneity is one explanation for this and indeed has been observed directly in at least one lipid binding site [68]. Nevertheless, the possibility of inadequate refinement

Table 5
Order parameter distribution of lipid chain segments for phospho-/glycolipids in crystals of transmembrane proteins [54][a]

Lipid[b]	Protein	$\langle S_{mol}\rangle$	$\langle(S_{mol}-\langle S_{mol}\rangle)^2\rangle^{1/2}$	N[c]
Ste_2PtdEtn	CO/*Rb. sphaeroides*	0.260	0.442	384
Ptd_2Gro, PtdCho, (GlcGal)Gro	RC/*Rb. sphaeroides*	0.235	0.522	89
PtdEtn, PtdCho, PtdIns, Ptd_2Gro	CR/*S. cerevisiae*	0.186	0.466	123
Ole_2PtdCho	cyt b_6f/*M. laminosus*	0.152	0.474	128
Phy_2Gro	bR/*H. salinarum*	0.587	0.399	96
Phy_2Gro	bR/*H. salinarum*	0.444	0.462	234

[a] $\langle S_{mol}\rangle$ is the mean order parameter of the different chain segments (S_{mol}=$S_{ZZ}S_{z'z'}$) and $\langle(S_{mol}-\langle S_{mol}\rangle)^2\rangle$=$\langle S_{mol}^2\rangle-\langle S_{mol}\rangle^2$ is the mean squared width of the order parameter distribution.

[b] See Table 1 for references.

[c] Total number of chain segments.

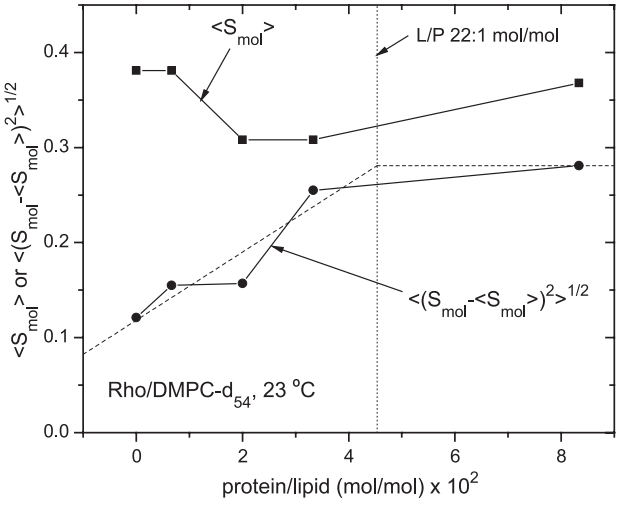

Fig. 8. Dependence on protein/lipid ratio of the mean order parameter $\langle S_{mol}\rangle$ (■) and width $\langle(S_{mol}-\langle S_{mol}\rangle)^2\rangle^{1/2}$ (●) of the order parameter distribution of the lipid chains in recombinants of bovine rhodopsin with [$^2H_{54}$]-myr$_2$PtdCho in the fluid phase at 23 °C (data from Ref. [11]).

[60] must also be considered. Perhaps it is significant to note in this connection that the disorder of palmitoyl-oleoyl phosphatidylcholine in a molecular dynamics simulation of lipids with a bacteriorhodopsin model structure (Refs. [69,70]) is associated with staggered, not eclipsed, chain conformations. For eight of the lipids that contact the protein directly, the conformational populations (n>3) are 79% *trans*, 13% *gauche*, 4% *skew* and 4% *cis*, where the latter is accounted for entirely by the 9,10 double bond of the oleoyl chains.

It is worth noting here that one expects chain order parameters to be specified more reliably in the crystal structures than are the individual torsion angles. This is because the chain segment orientation is defined along the direction of the chain long axis, i.e., that of the principal crystallographic electron density. Therefore, more reliance can be put on the segmental order parameters than on the detailed chain conformations.

Configurational disorder and heterogeneity appear to be general features of protein-interacting lipids in crystals [54]. With the possible exception of bacteriorhodopsin, there is little evidence for pronounced ordering of lipid chains that has been a feature of some hard-wall simulations of lipid–protein interactions. Further, it is not possible to invoke lipid chain entropy as a driving force for assembly of protein transmembrane domains, as has been done occasionally. At least some of the lipids resolved in protein crystals—those in well-defined clefts or at the interface between subunits, such as the phosphatidylethanolamines associated with *Rb. sphaeroides* cytochrome oxidase [13]—are located at specific sites, and therefore may have more narrowly defined configurations than those that are not resolved crystallographically. Energetically favourable hydrophobic matching with the fluid lipid milieu may be achieved better by these unresolved lipids. Additionally, some chain segments of lipids that are not in the first shell may, nonetheless, contact parts of the apolar surface of the protein.

4. Single proteins

This section deals with various different aspects of lipid–protein interactions studied by spin-label EPR that were not included in the previous review [4]. These comprise: the unusual specificity of bovine seminal plasma proteins for phosphatidylcholine; the action of local anaesthetics at the lipid–protein interface of the nAcChoR; the role of lipids in oligomerisation of the cardiac regulatory protein phospholamban; and the characterisation of avidin/biotin-lipid conjugates as a model for glycosylphosphatidylinositol (GPI)-linked proteins and other proteins with covalently linked chains.

4.1. PDC-109 and phosphatidylcholine membranes

Binding of PDC-109—a mixture of glycosylated and nonglycosylated forms of the major protein in bovine seminal plasma—to the sperm plasma membrane results in an efflux of cholesterol and choline phospholipids, a necessary event before capacitation of the sperm can occur [71,72]. The protein consists of an acidic N-terminal followed by two tandemly repeating fibronectin type-II (Fn-II) domains. Each Fn-II domain contains two extended regions that are predicted to have favourable free energy of transfer to the interfacial region of a lipid membrane (see Fig. 9). Only relatively short sections of these regions,

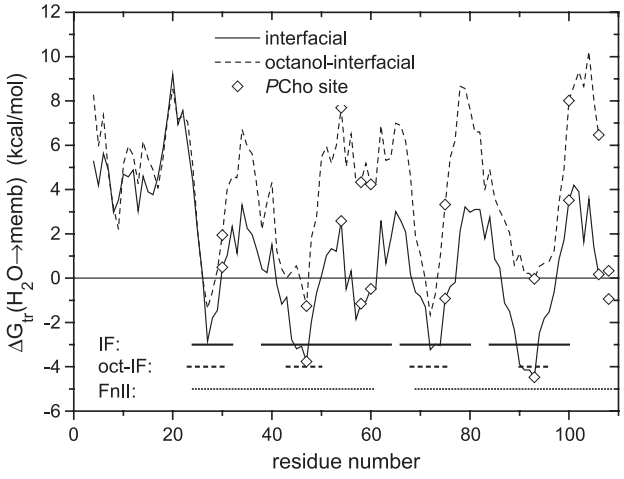

Fig. 9. Hydropathy profile for PDC-109, calculated with the interfacial (solid line) and octanol-minus-interfacial (dashed line) hydrophobicity scales of White and Wimley [73]. Plotted is the free energy of transfer from water to the membrane interface (solid line) and from the interface to the hydrophobic core of the membrane (dashed line), by using a seven-residue window. Solid and dashed horizontal lines represent energetically favourable regions for transfer to the membrane interface (IF) and to the hydrophobic core (oct-IF), respectively. Dotted horizontal lines designate the two FnII domains. Diamonds represent the five aromatic residues that form the two phosphocholine binding sites [74].

however, are predicted to penetrate the hydrophobic core of the membrane, as reflected by the octanol-minus-interfacial hydrophobicity scale.

Lipid interactions with PDC-109 are of considerable interest because, in contrast to integral membrane proteins [4], it displays a marked specificity for the zwitterionic phospholipid, phosphatidylcholine [75]. In view of the ubiquitous presence of phosphatidylcholines (or sphingomyelin) in mammalian membranes, proteins that interact with choline lipids are important not only from a structural and functional standpoint, but also with regard to possible pathologies that might arise from specific protein or peptide interactions with these major membrane constituents.

4.1.1. Lipid selectivity of PDC-109

Fig. 10 shows the EPR spectra of different phospholipids spin-labelled on the 14-C atom of the *sn*-2 chain, and of two steroid-based spin-labels, in bilayer vesicles of dimyristoyl phosphatidylcholine (myr_2PtdCho) to which PDC-109 has been added. The spectra, all recorded in the fluid phase of myr_2PtdCho, consist of two components, just as is found with these lipid labels interacting with integral transmembrane proteins. One component in the spectrum is similar to the fluid lipid spectrum from bilayer membranes (shown by the dashed line). The second component (resolved in the outer wings of the spectrum) has a much larger outer hyperfine splitting and represents a lipid population whose acyl chains are in direct contact with the protein. Experiments with phosphatidylcholine spin-labelled higher up the *sn*-2 chain indicate motional restriction by protein–lipid interaction throughout its entire length [76,77].

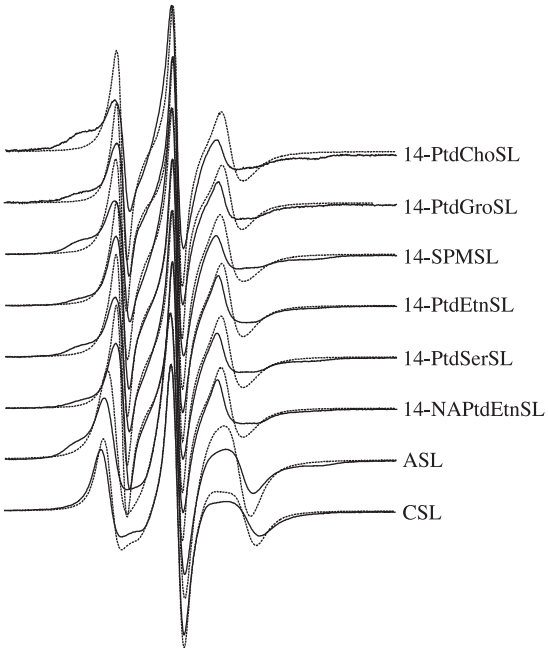

Fig. 10. EPR spectra of different spin-labelled lipids in the fluid phase of myr_2PtdCho membranes (· · · · · · · · ·) and of myr_2PtdCho/PDC-109 (lipid/protein, 1:2 w/w) recombinants (—). Phospholipids with the spin-label on the 14 C-atom of the *sn*-2 chain are: 14-PtdChoSL (phosphatidylcholine), 14-PtdGroSL (phosphatidylglycerol), 14-SPMSL (sphingomyelin), 14-PtdEtnSL (phosphatidylethanolamine), 14-PtdSerSL (phosphatidylserine), 14-NAPtdEtnSL (*N*-acyl phosphatidylethanolamine), as well as the cholestane spin-label (CSL) and androstanol spin-label (ASL). T=28 °C. The spectral width is 10 mT [76].

Table 6
Selectivity, (K_r/K_r^{PC}), of lipid interaction with PDC-109 in complexes with myr_2PtdCho and effect of 20 mol% cholesterol, $(N_b/n_t)/(N_b/n_t)_o$ [76,78]

Lipid spin-label	K_r/K_r^{PC}	$(N_b/n_t)/(N_b/n_t)_o$[a]
PtdCho	1.0	1.6
SPM (Cer*P*Cho)	1.0	1.5
PtdH (pH 8.5)	1.4	–
PtdH (pH 6.0)	0.96	–
PtdGro	0.61	–
PtdSer	0.61	1.6
PtdEtn	0.34	1.7
N-acylPtdEtn	0.30	–
ASL	0.61	1.5

[a] Ratio of the number of motionally restricted lipids, N_b, to the lipid/protein binding stoichiometry, n_t, in the presence of cholesterol to that [viz., $(N_b/n_t)_o$] in the absence of cholesterol (i.e., for PDC-109/myr_2PtdCho alone). See Ref. [78].

The relative amounts of the fluid and motionally restricted spectral components in Fig. 10 differ between the different lipid species, reflecting the selectivity of interaction with the PDC-109 protein. Table 6 lists the relative association constants, K_r, for the different lipids, normalised to those for phosphatidylcholine, K_r^{PC}. These establish a lipid selectivity for interaction with PDC-109 that is in the order phosphatidic acid (Ptd, pH 8.5)> phosphatidylcholine (PtdCho) ≈ sphingomyelin (SPM) ⩾ phosphatidic acid (PtdH, pH 6.0)>phosphatidylglycerol (PtdGro) ≈ phosphatidylserine (PtdSer) ≈ androstanol (ASL)>phosphatidylethanolamine (PtdEtn) ⩾ *N*-acyl phosphatidylethanolamine (*N*-acylPtdEtn) ≫ cholestane (CSL) [76]. With the exception of phosphatidic acid at high pH, the selectivity of PDC-109 is highest for the choline-containing phospholipids phosphatidylcholine and sphingomyelin. This is a highly unusual situation compared with spin-label results obtained on selectivity of lipid interaction with integral membrane proteins [4], where choline phospholipids show little specificity.

The results on interaction with lipid probes in phosphatidylcholine membrane vesicles are in agreement with earlier experiments on binding of PDC-109 to different phospholipids coated on plastic plates [75]. Under the conditions of the EPR spin-label experiments (lipid/protein 2:1 w/w), the lipid vesicles are completely solubilised by PDC-109 producing lipid–protein micelles [76], a result that undoubtedly is related to the ability of PDC-109 to induce cholesterol efflux from the sperm cell membrane.

4.1.2. Lipid stoichiometry of PDC-109

At saturation binding of PDC-109 to myr_2PtdCho (i.e., 2:1 w/w), the stoichiometry of the motionally

restricted 14-PtdChoSL is rather low and corresponds to ~5–6 mol/mol. Evidently, only part of the protein directly contacts the lipids. A stoichiometry of ~11 motionally restricted lipids is obtained at low protein/lipid ratio with a short *sn*-2 chain spin-labelled phosphatidylcholine, assuming that all spin-labels contact PCD-109 more or less directly [79]. The short *sn*-2 chain PtdCho spin-label is also motionally restricted (to approx. 50%) by interaction with PDC-109 in bovine epididymal sperm cells [77]. Fluorescence titration at super-solubilising protein/lipid ratios yields a stoichiometry of ~12 myr$_2$PtdCho/PDC-109 [80], and ~10 PtdCho/PDC-109 in 2:1 mixtures with phosphatidylethanolamine or phosphatidylserine [79]. Also turbidity measurements yield an interpolated stoichiometry of 11 myr$_2$PtdCho/PDC-109 for solubilisation [76].

4.1.3. Cholesterol potentiation of PDC-109 interactions

Introduction of cholesterol into membranes of myr$_2$PtdCho increases the population of motionally restricted lipids induced by PDC-109 at saturation binding [78]. The pattern of lipid selectivity does not change from that found in the absence of cholesterol. This suggests that either the stoichiometry of lipid association sites (N_b), or the amount ($1/n_t$) of protein bound, increases for cholesterol-containing membranes. The final column in Table 6 gives the ratio of N_b/n_t for membranes containing 20 mol% cholesterol, to that for membranes of myr$_2$PtdCho alone. Because fluorescence titrations have detected no changes by cholesterol in protein binding at saturation [80], the values in Table 6 most probably reflect an increase in number, N_b, of lipid association sites in the presence of cholesterol.

The sterol, spin-labelled androstanol, is also motionally restricted by interaction with the PDC-109 protein (see Table 6). The same holds true for a spin-labelled analogue of cholesterol [81]. However, the affinity for the spin-labelled sterol is less than that for spin-labelled PtdCho. Also, the sterols require binding of PDC-109 to PtdCho vesicles for their interaction, because relatively little spin-labelled cholesterol is motionally restricted in vesicles of PtdSer or PtdEtn/PtdCho 1:1 mol/mol [81].

4.2. Nicotinic acetylcholine receptor and local anaesthetics

The nAcChoR is a ligand-gated sodium channel that effects post-synaptic transmission at the neuromuscular junction. The receptor is a heteropentamer, $\alpha_2\beta\gamma\delta$, composed of four different subunits, all of which surround the channel and contact membrane lipid (see Fig. 11, upper panel). Local anaesthetics, including tetracaine, procaine, benzocaine and also free fatty acids [82], function as noncompetitive blockers of the ion channel, i.e., operate at a site other than that for cholinergic agonists. Because of their large number and relatively low affinity, it was concluded that these noncompetitive sites

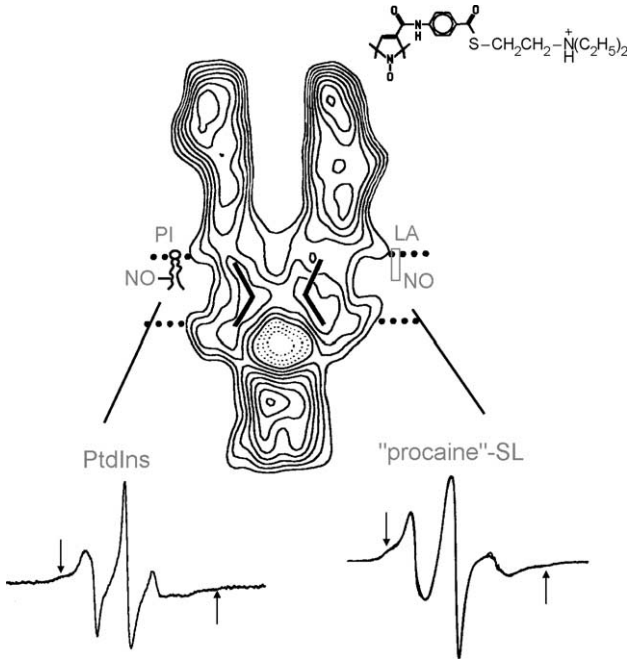

Fig. 11. Upper: electron crystallographic profile of the nAcChoR channel viewed from within the membrane plane [49]. The synapse is at the top and the cytoplasm at the bottom. The location of spin-labelled phosphatidylinositol (PI) and local anaesthetic (LA) at the protein–lipid interface is indicated schematically. Lower: EPR spectrum of: *left:* spin-labelled phosphatidylinositol (14-PtdInsSL) [86]; and right: spin-labelled derivative of procaine thioester (chemical structure in upper panel) [93] in nAcChoR-rich membranes from *T. marmorata*, T=22 °C. Total scan width=10 mT. Vertical arrows indicate the motionally restricted, protein-interacting spin-label component in each spectrum.

are located at the protein–lipid interface, within the membrane [83].

4.2.1. Lipid–protein stoichiometry and selectivity of nAcChoR

Spin-label EPR has demonstrated the association of fatty acids and the sterol androstanol at the lipid–protein interface in nAcChoR-rich membranes isolated from *Torpedo marmorata* electroplax [84]. This was subsequently extended to identify the spin-labelled phospholipid populations at the lipid–protein interface [33,85]. The lipid interaction stoichiometry for nAcChoR reconstituted in dioleoyl phosphatidylcholine (ole$_2$PtdCho) is 38–46 lipids/protein [33]. That estimated in native nAcChoR-rich membranes is 42±7 lipid sites/268 kDa protein [86]. Recent electron crystallography has shown that the intramembranous domain of the nAcChoR comprises a pentagonal arrangement of four-helix bundles [87]. The number of lipid chains that can be accommodated around the electron crystallographic cross-sections [49] is approximately 40 at the middle of the synaptic leaflet of the bilayer, and 50 at the level of the phospholipid headgroups in the cytoplasmic leaflet [86] (cf. Fig. 11, upper). For the two bilayer leaflets, this corresponds to 40–50 diacyl lipids (or cholesterol, which has a comparable cross-section) per

receptor, in fair agreement with the motionally restricted lipid stoichiometry obtained from spin-label EPR. Molecular modelling, described in Section 2 [42], reveals that ca. 52±4 diacyl lipids can be accommodated around the perimeter of the nAcChoR structure solved by Miyazawa et al. [87], which somewhat exceeds the stoichiometry of motionally restricted lipids.

Lipids interacting with the nAcChoR may be divided into a high-specificity group consisting of stearic acid, androstanol, cardiolipin (Ptd_2Gro), phosphatidic acid (PtdH) and phosphatidylinositol (PtdIns); an intermediate group consisting of phosphatidylserine (PtdSer) and phosphatidylglycerol (PtdGro); and a low-specificity group consisting of phosphatidylcholine (PtdCho), phosphatidylethanolamine (PtdEtn) and cholestane [33,86]. The selectivity for negatively charged phospholipids correlates with the obligate requirement for anionic lipid, in addition to a neutral lipid component such as cholesterol, to obtain effective reconstitution [88,89]. In particular, the agonist-induced ion flux response was found to be in the ratio 1:0.7:0.4 for PtdCho/cholesterol vesicles containing 20 mol% PtdH, Ptd_2Gro and PtdSer, respectively [89]. Interestingly, the gangliosides G_{D1b}, G_{M1}, G_{M2} and G_{M3} display no selectivity relative to PtdCho for the nAcChoR [86]. They thus belong to the low specificity group of lipids, but are not excluded absolutely from interaction with the receptor.

4.2.2. Spin-labelled local anaesthetics interacting with nAcChoR

Spin-labelled analogues of intracaine [90] and of procaine [91] have been shown to be capable of blocking sodium conduction in nerve. Additionally, spin-labelled fatty acids have been found to exhibit local anaesthetic potency with the nAcChoR [92].

The EPR spectrum of spin-labelled procaine thioester in nAcChoR-rich membranes from *T. marmorata* is shown at the lower right of Fig. 11. The chemical structure of this spin-labelled local anaesthetic is shown at the upper right of the figure. As for spin-labelled phospholipids, the EPR spectrum of spin-labelled thioprocaine consists of two components. One component is identical to that of the spin-label in fluid bilayer membranes of the extracted membrane lipids. The second component (indicated by the vertical arrows in Fig. 11) corresponds to spin-labelled anaesthetic molecules undergoing restricted motion at the lipid–protein interface. All spin-labelled local anaesthetic analogues tested display a selectivity, relative to phosphatidylcholine, for interaction with the AcChoR protein [93]. The rightmost column of Table 7 gives the relative association constants, K_r^{LA}, for spin-labelled derivatives of procaine and benzocaine, and for a spin-labelled analogue of tetracaine. In each case, the attachment of the spin-label nitroxyl ring is that indicated at the top right of Fig. 11. Generally speaking, the spin-labelled local anaesthetics can be divided into three groups with respect to their selectivity for the nAcChoR: a high specificity group, such as the thioprocaine and benzocaine derivatives, with $K_r^{LA}/K_r^{PC}>2$; medium specificity anaesthetics, such as the procainamide derivative and tetracaine analogue with $K_r^{LA}/K_r^{PC}\sim1.6–1.9$; and low-specificity anaesthetics, such as the procaine derivative, with $K_r^{LA}/K_r^{PC}\leqslant1.3$ [93].

Table 7
Relative association constant of phosphatidylinositol (PI) in nAcChoR-rich membranes from *T. marmorata* in the presence, $K_r^{PI}(LA)$, and absence, $K_r^{PI}(0)$, of 0.2 mg/ml local anaesthetics (LA) [86], and relative association constants, K_r^{LA}, of spin-labelled local anaesthetic analogues in nAcChoR-rich membranes [93]

LA additive	$K_r^{PI}(0)/K_r^{PI}(LA)$	LA spin-label	$K_r^{LA}(0)/K_r^{PC}(0)$[a]
–	1.0	PC	1.0
+Tetracaine	2.2	"tetracaine"	1.9
+Procaine	1.5	"procaine"	1.3
+Benzocaine	1.4	"benzocaine"	2.3

[a] Normalised to the relative association constant for phosphatidylcholine (PC). All measurements in the absence of unlabelled LA.

In a way similar to that for the titratable anionic phospholipids (see Ref. [4]), the population of cationic procaine and thioprocaine local anaesthetics that is associated with the protein depends on the pH and ionic strength [93]. Only in the uncharged form or in the charged form at high ionic strength do these two derivatives express a selectivity of interaction relative to that of phosphatidylcholine (i.e., $K_r^{LA}/K_r^{PC}>1$). On the other hand, the specificity of the benzocaine derivative, which lacks the basic side chain, is unaffected by changes in pH and ionic strength. Corresponding differences are found both in steady-state pharmacological effects and in rates of action, between aminated local anaesthetics in their uncharged deprotonated forms and the cationic protonated forms [94]. Of course, pH titration also affects the partitioning of these anaesthetics into the lipid milieu of the membrane [95].

4.2.3. Competition between local anaesthetics and lipids for nAcChoR sites

The overlap between the association sites for local anaesthetics and those for phospholipids at the protein–lipid interface in nAcChoR-rich membranes is revealed by competition experiments [86]. The fraction of spin-labelled phosphatidylinositol that is motionally restricted (indicated by the vertical arrows at the lower left of Fig. 11) is reduced on addition of authentic (i.e., unlabelled) local anaesthetics. The extent of displacement of spin-labelled PtdIns from the lipid–protein interface varies with the different local anaesthetics. The left-hand columns of Table 7 give the results of competition experiments. The ratio, $K_r(0)/K_r(LA)$, of the association constant for PtdIns in the absence of local anaesthetic to that in the presence of local anaesthetic is related directly to the relative association constant for the unlabelled local anaesthetic itself. Although the relative order differs, the values of $K_r^{PI}(0)/K_r^{PI}(LA)$ are comparable in size to the relative association constants, K_r^{LA}/K_r^{PC} of the spin-labelled local anaesthetics

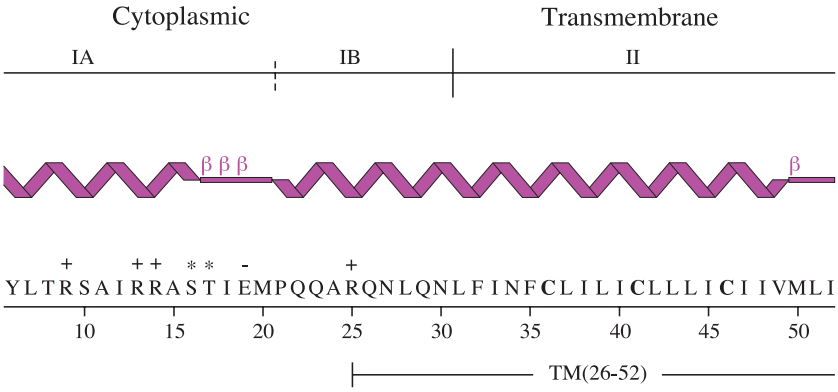

Fig. 12. Amino acid sequence of rabbit heart phospholamban. Charged residues are indicated by +,− and phosphorylation sites by asterisks. Secondary structure cartoon corresponds to C41F-pig heart phospholamban in chloroform-methanol [97]. Region marked βββ is a type III turn. Domain IA contains an amphipathic helix and the regulatory phosphorylation sites. Domain IB follows the hinge region and contains a high proportion of amidated residues. Domain II is hydrophobic and constitutes a single transmembrane helix.

(Table 7). The pattern for association of the different local anaesthetics is probably modified by substitution with the spin-label group, most particularly by removing the C_4 alkyl chain of tetracaine.

Interestingly, the local anaesthetics are not able to compete so effectively with spin-labelled stearic acid as they do with the spin-labelled phospholipid, PtdIns [86]. The effect of the local anaesthetics therefore is not simply one of electrostatic competition at the protein surface, as also can be inferred from the partial displacement of PtdIns by benzocaine. The different degrees of displacement for the two types of spin-labelled lipid further support the proposal that additional sites for fatty acids exist at the intramembranous surface of the receptor, which are different from those for phospholipids [96]. The most recent electron crystallographic model of the nAcChoR channel suggests that alcohols and anaesthetics might bind in water-filled spaces behind the pore-lining M2 helices [87]. The spin-label results indicate that local anaesthetics can also occupy phospholipid sites. Tetracaine, at least, can occupy sites taken up by fatty acid because this spin-labelled lipid was displaced partially. It is possible that there is no very clear distinction between phospholipid and local anaesthetic sites at the hydrophobic surface of the protein, or at least that some sites may overlap.

4.3. Oligomer formation of phospholamban

Phospholamban (PLB) is a 52-residue transmembrane protein (see Fig. 12) that exerts a phosphorylation-dependent regulatory effect on the cardiac calcium pump. The functionally active form is the monomer, but the protein has a strong tendency to oligomerise and it has been suggested that the pentamer may be a storage form [98,99]. Clearly, the aggregation state of the protein in the membrane is a matter of considerable functional interest. Mutation of the three cysteine residues in PLB to alanine leads to loss of pentamer formation in SDS [100].

EPR of spin-labelled lipids provides a ready means for investigating the oligomerisation state of PLB, via the influence on the stoichiometry, $N_b^{(1)}$, per monomer of the perimeter lipids [40,101]. The geometric model for helix packing that is given in Section 2 relates the ideal stoichiometry per monomer, $N_b^{(1)}$, to the number of transmembrane helices, n_α, i.e., to the oligomer size [41]:

$$N_b^{(1)} = \frac{\pi}{n_\alpha}\left(\frac{D_\alpha}{d_{ch}} + 1\right) + \frac{D_\alpha}{d_{ch}} \quad (9)$$

which is the version of Eq. (5) that is appropriate to bitopic, i.e., single-helix, monomers. Table 8 lists the stoichiometry

Table 8
Stoichiometries ($N_b^{(1)}$) of lipid–protein interactions, and degree of oligomerisation (n_α), for phospholamban (PLB) and transmembrane peptide (TM) mutants in different lipid hosts

Protein	Lipid	$N_b^{(1)}$ (mol/mol)	n_α	Reference
PLB (WT)	ole$_2$PtdCho	5.6±0.5	3.5±0.4	[40]
PLB (L37A)	ole$_2$PtdCho	12±0.5	1.15±0.15	[40]
PLB (C36A, C41A, C46A)	myr$_2$PtdCho	7.1±0.2	1.9±0.1	[102]
	pal-olePtdCho	4.0±0.1	4.9±0.1	[102]
	myr$_2$PtdGro	11.3	1.0	[102]
	ole$_2$PtdCho	7.8±0.3	2.2±0.5	[101]
TM$^{26–52}$ (C36A, C41A, C46A)	myr$_2$PtdCho	4.0±0.2	5.1±0.6	[102]
	pal-olePtdCho	4.0±0.2	5.0±0.5	[102]
	myr$_2$PtdGro	10.1±1.3	1.2±0.2	[102]
	ole$_2$PtdCho	6.0±0.6	3.3±0.4	[101]

of motionally restricted lipids and values derived for the degree of oligomerisation, n_α, for wild-type (WT) PLB and two mutants, as well as for the transmembrane section (TM, residues 26–52) of PLB, in different lipid hosts.

Wild-type PLB and its TM section in ole$_2$PtdCho have an intermediate degree of oligomerisation that could represent a mixture of monomer and pentamer [40]. A single-residue mutation L37A in the helix contact region converts PLB in ole$_2$PtdCho to the monomer. The cysteine-less mutant of PLB is monomeric in the anionic lipid myr$_2$PtdGro, but is on average dimeric in the corresponding phosphatidylcholine myr$_2$PtdCho. In the unsaturated lipid pal-olePtdCho, the cysteine-less mutant becomes pentameric. In ole$_2$PtdCho, however, an intermediate mean degree of oligomerisation is obtained (but note that measurements in ole$_2$PtdCho were made at 0 °C, whereas those in all other lipids were at 30 °C). The TM peptide is pentameric in both myr$_2$PtdCho and pal-olePtdCho, and only in the anionic lipid myr$_2$PtdGro is it monomeric. This suggests that pentamer formation is driven by favourable knobs-into-holes packing of the transmembrane domains, which is destabilised by electrostatic repulsion between the charged cytoplasmic domains [101].

The monomeric stoichiometry found for the L37A mutant, and for PLB (C36,41,46A) in myr$_2$PtdGro, is significant. It is far from self-evident that a single transmembrane α-helix would provide a sufficiently extensive hydrophobic face to induce a motional restriction of the lipid chains such as is produced by large integral proteins. Simple alternating leucine-alanine transmembrane α-helices that are flanked by tryptophan or lysine do not induce a motionally restricted spin-labelled lipid population [103,104], nor does the single hydrophobic helix of the lung surfactant protein SP-C [105]. The phospholamban monomer therefore has a particular intramembranous sequence that is able to support motional restriction of adjacent lipids. Possibly this feature also contributes to the propensity for helix–helix interactions, but is not so susceptible to specific disruption by mutation of single residues as in the latter case.

4.4. Avidin/biotin–lipid conjugates

The binding of biotin to avidin is one of the highest affinity interactions known in biology; dissociation is totally negligible over the time scale of any experiment [106]. For this reason, avidin (or streptavidin) bound to the biotinylated headgroup of phosphatidylethanolamine (see e.g., Ref. [107]) serves as a model for covalent lipid anchors of membrane-associated proteins (e.g., GPI-linked proteins). Also, because phospholipases must bind to the lipid headgroups (e.g., Ref. [108]), the avidin/biotin-PtdEtn system models certain aspects of their interaction with lipids.

The mode of membrane-anchoring of water-soluble avidin was studied by using biotin-phosphatidylethanolamines that are spin-labelled at different positions in their *sn*-2 chain [109]. The spin-labelled biotin-PtdEtn was incorporated at low concentration (1 mol%) in inert PtdCho membranes to which avidin does not bind. Fig. 13 shows the lipid chain flexibility profile, as a function of position n of spin-labelling, that is registered by the outer hyperfine splitting, $2A_{max}$, in the EPR spectra of the various spin-label positional isomers. In the absence of avidin, a systematic decrease in A_{max} is found as the spin-label is stepped down the chain towards the centre of the membrane. Generally speaking, this is a measure of the angular amplitude of motional freedom of the spin-labelled lipid chain segment, and is a characteristic signature of fluid bilayer membranes. The chain flexibility gradient is preserved on binding avidin to the biotin headgroup, but the overall size of A_{max} increases dramatically. This direct and highly specific effect of protein binding corresponds to an upward shift in the flexibility profile by ~7 CH_2 units (see Fig. 13), which translates to an upward displacement of the biotin-PtdEtn by 0.7–0.8 nm, relative to the PtdCho membrane. Electron crystallography on two-dimensional arrays of homologous streptavidin bound to biotin-PtdEtn monolayers has found that the carboxyl group of the bound biotin is located ~0.8 nm from the surface of the underlying lipid layer [111], as indicated

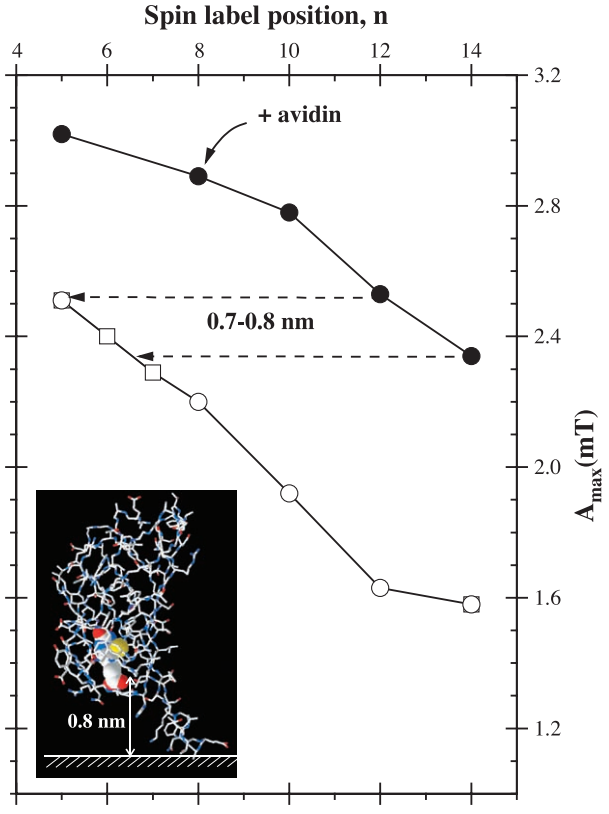

Fig. 13. Spin-labelled *N*-biotinyl phosphatidylethanolamine, with (filled circles) and without (open circles) bound avidin, in dimyristoyl phosphatidylcholine membranes. Spin-label outer hyperfine splitting constant, A_{max}, is plotted against spin-label position, n, in the *sn*-2 chain (data from Ref. [109]). Inset: the structure of biotin-bound streptavidin from PDB:1STP [110]. The location of the lipid surface is approximately that determined in Ref. [111].

Table 9
Enhancement in T_1T_2-relaxation rate, ΔR ($10^{13}\times s^{-2}$), of spin-labelled biotin-PtdEtn (n-BPtdEtnSL) by aqueous Ni^{2+} ions, by membrane-saturated molecular oxygen and by spin-labelled PtdCho, in the presence and absence of bound avidin [112]

n-BPtdEtnSL	Relaxant	−Avidin	+Avidin
n=8	30 mM Ni^{2+}	8.5	10.5
n=8	saturating O_2	16.5	4.0
n=12	12-PtdChoSL	4.0	1.6

schematically by the insert in Fig. 13. This is consistent with the vertical movement deduced from the EPR studies.

Direct evidence for an upward vertical displacement of the biotin-PtdEtn on complexation with avidin comes from EPR measurements of spin-label T_1-relaxation enhancement induced by differentially located paramagnetic species [112]. Table 9 shows that the relaxation enhancement, ΔR, of spin-labelled biotin-PtdEtn by aqueous Ni^{2+} ions is increased by 24%. That by molecular oxygen, which is preferentially concentrated within the membrane, is decreased by 76%, and that by membrane-bound spin-labelled PtdCho is correspondingly decreased by 60%. The ratio of aqueous to intramembrane enhancements is increased approximately 5-fold by the upward movement of biotin-PtdEtn on binding avidin to the polar headgroup.

This type of vertical displacement is likely to be a general feature of the interaction with proteins, e.g., cholera toxin or anti-cardiolipin antibodies, that bind to lipid headgroups. The enzymes of phospholipid hydrolysis are a further class of examples. In phospholipase A_2, the active site is located ~1.5 nm from the protein surface [108]. A movement of the phospholipid substrate out of the membrane, through a hydrophobic channel that leads to the catalytic site, is therefore required for the enzymatic hydrolysis.

5. Integral protein/peripheral protein couples

Lipid interactions with single integral proteins have been reviewed previously [4] and in the preceding section. A considerable body of spin-label EPR work also exists on lipid interactions with single peripheral proteins. Some of this latter work was reviewed in Refs. [113,114]. Far fewer spin-label studies have been undertaken on the mutual interactions of integral and peripheral proteins in defined reconstituted systems. This section is devoted specifically to this aspect of protein–lipid interactions, including protein-linked lipid chains. The cytochrome c/cytochrome oxidase and myelin basic protein/myelin proteolipid couples are treated here, followed by lipid-linked avidin interacting with the proteolipid protein.

5.1. Cytochrome c/cytochrome oxidase couple

Cytochrome c oxidase is a large, multi-subunit integral protein and its redox substrate cytochrome c is a small basic, water-soluble peripheral membrane protein. Lipid–protein interactions have been characterised previously for each protein separately by spin-label EPR methods. Bovine and yeast cytochrome oxidase motionally restrict $N_b \approx 55$ PtdCho lipids per 200 kDa protein at the intramembranous surface [32], and display a selectivity for negatively charged lipids, particularly cardiolipin [115,116]. Cytochrome c binds to negatively charged lipid membranes at a level of ca. nine lipids/protein at saturation [113,117], without appreciable penetration into the hydrophobic core of the membrane [118].

Bovine cytochrome c oxidase reconstituted in the anionic lipid dimyristoyl phosphatidylglycerol (myr_2PtdGro) also motionally restricts $N_b^o \approx 55$ lipids [119], a stoichiometry in agreement with that obtained in the zwitterionic lipid myr_2PtdCho. Binding of cytochrome c increases the number of motionally restricted lipids per cytochrome oxidase, in the coupled system. Fig. 14 gives the population of motionally restricted lipid, normalised to cytochrome oxidase content, as a function of the total myr_2PtdGro/cytochrome oxidase ratio, n_t. In the absence of cytochrome

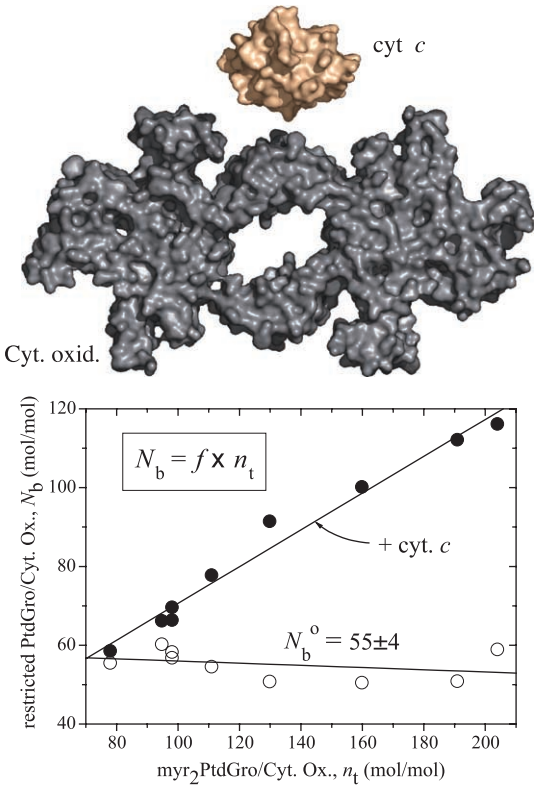

Fig. 14. Lower: number of motionally restricted lipids, N_b per cytochrome oxidase, in the absence (open circles) and presence (filled circles) of cytochrome c bound at saturation to reconstituted membranes with myr_2PtdGro/cytochrome oxidase ratios, n_t. ($N_b=f\times n_t$ where f is the fraction of motionally restricted spin-labelled PtdGro obtained from the EPR difference spectra.) (data from Ref. [119]). Upper: structure of the transmembrane domain of the cytochrome oxidase dimer is from PDB:1OCC [120], and of cytochrome c is from PDB:1AKK [121]. Orientation of cytochrome c at the membrane surface is that determined in Ref. [118] (figure produced with pyMOL; http://www.pymol.org.)

c the stoichiometry remains constant, but in the presence of saturating amounts of bound cytochrome *c* the motionally restricted lipid population increases progressively with the myr$_2$PtdGro/cytochrome oxidase ratio. The stoichiometry becomes greater, the greater is the cytochrome *c*/cytochrome oxidase ratio, at least up to the highest value of n_t given in Fig. 14.

The synergistic effect of cytochrome *c* can be rather large; the motionally restricted lipid population, per cytochrome oxidase, is more than doubled at the highest lipid/cytochrome oxidase ratio, n_t. It is therefore likely that surface-bound cytochrome *c* propagates the chain restriction induced by cytochrome oxidase to the second and possibly even third shell of lipids surrounding the protein. Cytochrome *c* binds without restriction to the myr$_2$PtdGro cytochrome oxidase membranes, including to the first shell of lipids directly in contact with cytochrome oxidase. Because it binds to about nine myr$_2$PtdGro molecules, it could thereby form a surface-bridge between lipids in the first and adjacent boundary shells (see molecular projections in Fig. 14). Such a propagation mechanism is possible because, although cytochrome *c* alone does not create a specific population of motionally restricted lipids, it does induce a generalised motional restriction of all anionic lipids to which it binds at saturation [117].

Cytochrome *c*, therefore, can induce formation of microdomains containing cytochrome oxidase in which the mobility of the lipid chains is appreciably restricted relative to that in fluid membranes. Comparison with the MBP-PLP couple (which is presented in the next section) suggests that preconditions for this mechanism are that the inducing protein binds the lipids directly contacting the integral protein, and possibly also that it does not itself penetrate the membrane. A qualitatively similar phenomenon is observed in the interaction of melittin with the Ca-ATPase and associated lipids in sarcoplasmic reticulum membranes [122].

5.2. Myelin basic protein/myelin proteolipid protein couple

The myelin proteolipid protein (PLP) is a relatively small hydrophobic protein that is thought to traverse the membrane as a four-helix bundle (see e.g., Ref. [123]). The myelin basic protein (MBP) is of comparable size to PLP, and has little structure in solution, but adopts α-helical and β-sheet conformations on binding to anionic membranes [124]. Together these two proteins constitute ~80% of the total protein in CNS myelin, where they are present in roughly equimolar quantities.

Double reconstitutions produced by binding MBP to myr$_2$PtdGro membranes that contain PLP, have been used to study the mutual protein–lipid interactions of the myelin integral and peripheral proteins [125]. Fig. 15 (on the left) shows the saturation binding stoichiometry of MBP (per lipid) as a function of PLP content in the membrane. Up to a critical PLP/myr$_2$PtdGro ratio, the binding of MBP is undisturbed by the presence of PLP. Beyond this critical content, the saturation binding of MBP decreases roughly linearly with PLP content, reaching zero at a myr$_2$PtdGro/PLP ratio of $N_1 \approx 11$ mol/mol. The latter corresponds also with the number of lipids $N_b \approx 11$ that are motionally

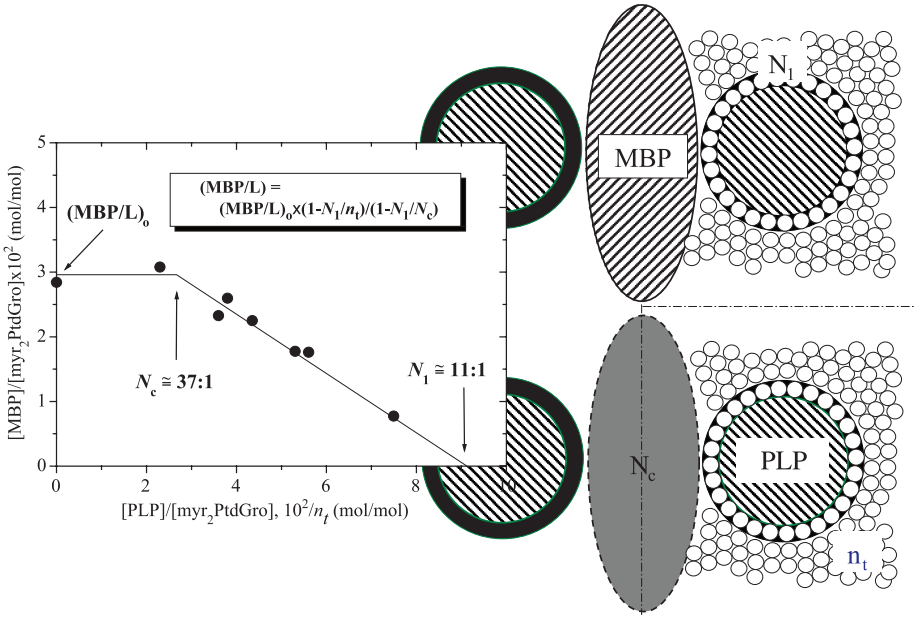

Fig. 15. Binding of the peripheral myelin basic protein (MBP) to myr$_2$PtdGro membranes containing the integral myelin proteolipid protein (PLP). A critical number of lipids, N_c per PLP that is indicated by the dark grey area, is required for undisturbed surface binding of MBP (right-side schematic). For total number of lipids per PLP $n_t<N_c$ (mol/mol), MBP binding decreases approximately linearly with $1/n_t$, reaching zero at a total lipid/PLP ratio $n_t=N_1$ (mol/mol) (left-side plot) (data from Ref. [125]).

restricted by PLP alone [35]. Apparently, this first boundary shell of lipids is unavailable for binding to MBP, once the PLP density in the membrane exceeds a critical value. The critical PLP content corresponds to a myr$_2$PtdGro/PLP ratio of $N_c \approx 37$ mol/mol. This also corresponds to the number of lipids interacting with MBP at surface saturation: 36 myr$_2$PtdGro/MBP [126]. Therefore, the minimum critical area of lipid surface between PLP assemblies that is required for undisturbed binding of MBP is comparable to the size of the basic protein itself. This simple situation of mutual steric exclusion between the two proteins is illustrated schematically on the right of Fig. 15. A phenomenological description of the decrease in MBP binding stoichiometry is possible, if proportionality to the total fraction of available lipids, viz., $(n_t - N_1)/n_t$, is assumed. This leads to the following expression [125]:

$$\frac{\mathrm{MBP}}{L} = \left(\frac{\mathrm{MBP}}{L}\right)_o \frac{(1 - N_1/n_t)}{(1 - N_1/N_c)} \qquad (10)$$

where $(\mathrm{MBP}/L)_o$ is the binding stoichiometry to myr$_2$PtdGro in the absence of PLP, and results in the functional dependence shown by the solid lines in Fig. 15.

Accompanying the mutual steric exclusion, saturation binding of MBP causes a 30–40% reduction in the stoichiometry of lipids interacting with PLP. This suggests that MBP disturbs the interaction of lipids with the intramembranous portion of PLP, quite possibly by means of the short membrane-penetrant portions of the peripheral protein. Unlike cytochrome *c*, MBP interacts directly with the lipid chains to a limited extent, in addition to the surface electrostatic association (see Ref. [126]). In this respect MBP resembles the precursor protein apocytochrome *c* [117]. This behaviour contrasts strongly with that of the cytochrome *c*/cytochrome oxidase couple, where binding of the peripheral protein enhances the motional restriction of the lipid shells surrounding the integral protein. Both this, and the striking difference in the influence of the integral protein on the extent that the peripheral protein binds, can be attributed to the difference in relative sizes of the partner proteins. The ratio of the number of lipids binding to MBP to the number of first-shell lipids motionally restricted by PLP is 36/11~3, whereas the corresponding ratio for cytochrome *c* and cytochrome oxidase is 9/55~0.2. With decreasing lipid content, steric interactions between cytochrome oxidase molecules become limiting before these can affect the binding of cytochrome *c* appreciably (indeed, for efficient electron transfer cytochrome oxidase must be fully accessible to cytochrome *c* at the rather high protein packing densities of the mitochondrial inner membrane).

In addition to steric exclusion between the two myelin proteins, there are also other mutual influences on the lipid–protein interactions. Table 10 [125] gives values for the increase in spectral anisotropy, ΔA_{max}, of spin-labelled PtdGro that is induced by saturation binding of MBP. This effect on lipid mobility is substantially attenuated in the presence of the proteolipid protein. At a myr$_2$PtdGro/PLP ratio of 25:1 mol/mol, the weakening of the MBP-myr$_2$PtdGro interaction is mostly a consequence of the reduced binding of MBP (cf. Fig. 15). At the lower myr$_2$PtdGro/PLP ratio, the lipid perturbation is reduced less, in spite of further decrease in MBP binding. This undoubtedly results from a mutual reinforcing of the lipid perturbation by both PLP and MBP, at high protein/lipid ratios. Notably, this latter effect is reduced considerably at higher ionic strength (100 mM NaCl), when binding of MBP is less.

Table 10
Increase in outer hyperfine splitting, ΔA_{max}, of phosphatidylglycerol spin-labelled at the 5-C atom of the *sn*-2 chain (5-PtdGroSL), on saturation binding of MBP to membranes of myr$_2$PtdGro containing the PLP

myr$_2$PtdGro/PLP (mol/mol)	ΔA_{max} ($10^{-4} \times T$)	
	10 mM NaCl	100 mM NaCl
1:0	3.6	3.3
25:1	1.0	0.7
17:1	2.3	1.2

Values are given for different ionic strengths (NaCl) of the suspending medium and T=30 °C.
Data from Ref. [125].

Table 11 gives the effect of MBP binding on the selectivity of lipid interactions with PLP. Selectivities of interaction with PLP (i.e., K_r/K_r^{PC}) are reduced for all spin-labelled lipids by binding of MBP, particularly for the negatively charged lipids. This weakening of the selectivity and modification of the selectivity ranking can be understood as a direct competition for the lipids by the two proteins. The relative association constants, K_r, for interaction of lipids with PLP that are given in Table 11 are defined relative to myr$_2$PtdGro as standard state in one case, but relative to myr$_2$PtdGro with MBP bound in the other.

It therefore seems that MBP and PLP (unlike cytochrome *c* and cytochrome oxidase) probably act independently, rather than synergistically, in their role in the compaction of nerve myelin. In particular, the double reconstitutions offer little evidence for the direct binding of MBP to PLP that has been suggested in some models.

5.3. Chain-linked avidin/proteolipid interactions

Interactions of protein-linked lipid chains with transmembrane proteins have been studied by using avidin/biotin-PtdEtn conjugates in membranes containing the myelin proteolipid [127]. Proteolipid (PLP or DM-20) was reconstituted in dimyristoyl phosphatidylcholine (myr$_2$PtdCho) membranes in which ca. 1 mol% biotin-PtdEtn spin-label was incorporated and bound by saturating quantities of avidin. Motionally restricted protein-linked chains were detected and quantitated by EPR spectroscopy.

Table 11
Relative association constants, K_r, of spin-labelled lipids with PLP in myr_2PtdGro membranes, with and without MBP

Lipid spin-label	K_r/K_r^{PC}		$\Delta\Delta G_L$ (kJ/mol)
	PLP	PLP+MBP	
SteH	2.9	2.3	0.6
Ptd_2Gro	3.0	2.7	0.3
PtdH	2.4	1.7	0.8
PtdGro	2.0	1.8	0.3
PtdSer	1.4	1.1	0.6
PtdEtn	1.7	1.2	0.9

K_r is normalised to the corresponding value, K_r^{PC}, for spin-labelled phosphatidylcholine.
$\Delta\Delta G_L$ is the increase in free energy of lipid association on binding MBP. Data from Ref. [125].

Data given in Table 12 show that spin-labelled biotin-PtdEtn alone displays a selectivity over phosphatidylcholine for interaction with the proteolipid protein. In part, this may be because biotin-PtdEtn is a negatively charged lipid. Saturation binding of avidin to the biotin-PtdEtn headgroups has rather dramatic effects that at first sight are perhaps somewhat surprising. It leads to a very substantial increase in the population of motionally restricted biotin-PtdEtn chains (see Table 12). Approximately 80% of the avidin-linked chains are restricted in membranes with a myr_2PtdCho/PLP molar ratio of n_t=37:1. This increased population, however, exhibits a lesser degree of chain motional restriction than is typical for first-shell boundary lipids, because it displays a steeper temperature dependence [127].

The relatively high effective stoichiometry of interaction can be explained when allowance is made for the closest interaction distance between the lipid-anchored avidin tetramer and the transmembrane proteolipid hexamers, without any specific interaction between the two types of membrane-associated proteins. As Fig. 16 indicates, the PLP hexamer and avidin tetramer are of comparable cross-sectional area, and the biotin-lipid binding sites are offset from the PLP–lipid interface by $r_p \approx 2.5$ nm [128]. At this distance, the number of lipids per PLP monomer that can be accommodated around the perimeter of the hexamer is given by the following extension of Eq. (5) [127]:

$$N_b' = \frac{\pi}{n_{agg}} \frac{(D_\alpha + 2r_p)}{d_{ch}} + \frac{n_\alpha D_\alpha}{d_{ch}} \quad (11)$$

where n_{agg}=6 is the aggregation number, and n_α=4 is the number of transmembrane helices per monomer, for PLP. This yields 15 perimeter lipids/monomer as compared with ca. 10 at the true boundary layer. In addition, the region of lipid bilayer that lies within this extended perimeter is inaccessible to the avidin-linked chains. This region corresponds to approximately half the cross-sectional area of avidin, i.e., to approximately 25 lipids per avidin tetramer, which translates into approximately 17 lipids per PLP monomer (see Refs. [107,127]). The effective lipid/protein ratio "seen" by the avidin-linked chains is reduced by this amount, and therefore the fraction of perimeter chains is given by f=15/(n_t−17)=0.75. This is close to the experimental values of f for 14-BPtdEtnSL that are given in Table 12. One may therefore conclude that, after the geometric extent of the lipid-anchored avidin is taken into account, it displays little selective interaction with the transmembrane proteolipid.

A major consequence of the above interpretation of the increased stoichiometry is that the avidin-linked chains are somewhat removed from the innermost protein–lipid interface. Nevertheless, their mobility is very markedly reduced relative to that in lipid membranes without transmembrane protein, although to a lesser extent than for freely diffusible first-shell lipids. The effects on the lipid chains of anchoring to avidin (which was discussed earlier in Section 4.4) render them far more susceptible to interactions and perturbations within the lipid matrix. This is demonstrated here by the interactions with an integral protein, but conceivably may

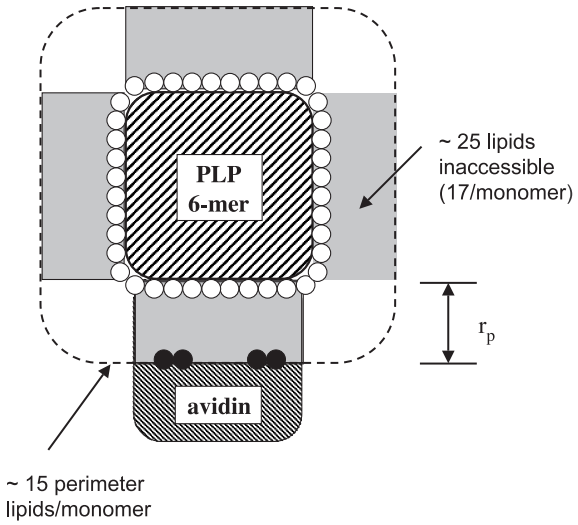

Fig. 16. Steric exclusion between the myelin proteolipid hexamer (PLP) and lipid-linked avidin tetramer. The avidin-linked chains (●) can approach only to within distance r_p (≈2.5 nm) of the PLP perimeter. The number of lipids, N_b, that can be accommodated at this distance is ≈15/PLP monomer (adapted from Ref. [127]).

Table 12
Fraction, f, of spin-labelled biotin-PtdEtn (14-BPtdEtnSL) or phosphatidylcholine (14-PtdChoSL), that is motionally restricted by interacting with PLP (or DM-20) in myr_2PtdCho membranes (lipid/protein=37:1 mol/mol), in the presence and absence of excess avidin

Protein	Spin-label	f	
		−Avidin	+Avidin
PLP	14-BPtdEtnSL	0.51	0.80
	14-PtdChoSL	0.29	–[a]
DM-20[b]	14-BPtdEtnSL	0.57	0.79
	14-PtdChoSL	0.30	–[a]

Data from Ref. [127].
[a] Avidin has no effect on 14-PtdChoSL in myr_2PtdCho membranes.
[b] DM-20 is the isoform of PLP in which residues 116–150 are deleted.

also extend to interactions with membrane lipids, in particular with the putative raft components sphingolipids and cholesterol.

5.4. Conclusions on protein couples

The interactions between the two peripheral/integral protein couples considered here differ greatly, being determined by the relative size of the two protein partners, and possibly also by their functional roles. Cytochrome *c* is much smaller than cytochrome oxidase and acts as a substrate of this multi-subunit redox-enzyme complex. The cytochrome associates intimately with its oxidase partner and both reinforces and propagates the influence of the integral protein on the chains of the surrounding lipids. Myelin basic protein and proteolipid protein are comparable in size and have a structural role in the compaction of nerve myelin. The interaction between these two membrane proteins is principally one of mutual steric exclusion. Although the interaction of avidin with the myelin proteolipid protein appears to be one of steric exclusion, the anchoring chains attached to avidin strongly sense the influence of the somewhat remote transmembrane sectors of the proteolipid protein. The above examples of synergistic interactions provide two rather different mechanisms for propagating lipid interactions induced by transmembrane proteins. Both are protein-driven and involve neither specifically cholesterol nor gel-phase lipid (cf. Ref. [129]). Nonetheless, both potentially could stabilise membrane microdomains and hence be operative in formation of putative sphingolipid membrane rafts [130].

6. Conclusion and outlook

Magnetic resonance methods, particularly those of spin-label EPR, continue to yield unique information on structural, dynamic and thermodynamic aspects of lipid–protein interactions, in membrane systems of increasing complexity. Crystal structures at higher resolution, and with improved refinement, should be able to settle open questions regarding conformational heterogeneity and specific versus nonspecific lipid association sites on the protein. In the future, increasing application of molecular dynamics simulations also should help further to resolve the potential dichotomy between dynamic membranes and static crystal structures.

Acknowledgements

We thank Frau I. Dreger for the preparation of the manuscript and figures. Our studies on lipid interactions with V-ATPases and the 16-kDa *Nephrops* protein are supported by the European Union (Contract No. QLGI-CT 2000-01801). DM and TP are members of the European COST D22 Action.

References

[1] D. Marsh, Experimental methods in spin-label spectral analysis, in: L.J. Berliner, J. Reuben (Eds.), Biological Magnetic Resonance, vol. 8, Plenum Publishing, New York, 1989, pp. 255–303.
[2] J.R. Brotherus, O.H. Griffith, M.O. Brotherus, P.C. Jost, J.R. Silvius, L.E. Hokin, Lipid–protein multiple binding equilibria in membranes, Biochemistry 20 (1981) 5261–5267.
[3] D. Marsh, ESR spin label studies of lipid–protein interactions, in: A. Watts, J.J.H.H.M. de Pont (Eds.), Progress in Protein–Lipid Interactions, vol. 1, Elsevier, Amsterdam, 1985, pp. 143–172.
[4] D. Marsh, L.I. Horváth, Structure, dynamics and composition of the lipid–protein interface. Perspectives from spin-labelling, Biochim. Biophys. Acta 1376 (1998) 267–296.
[5] R.D. Pates, D. Marsh, Lipid mobility and order in bovine rod outer segment disk membranes. A spin-label study of lipid–protein interactions, Biochemistry 26 (1987) 29–39.
[6] S.Y. Kang, H.S. Gutowsky, J.C. Hsung, R. Jacobs, T.E. King, D. Rice, E. Oldfield, Nuclear magnetic resonance investigation of the cytochrome oxidase-phospholipid interaction: a new model for boundary lipid, Biochemistry 18 (1979) 3257–3267.
[7] J. Seelig, A. Seelig, L. Tamm, Nuclear magnetic resonance and lipid–protein interactions, in: P.C. Jost, O.H. Griffith (Eds.), Lipid–Protein Interactions, vol. 2, John Wiley and Sons, New York, 1982, pp. 127–148.
[8] E. Oldfield, NMR of protein–lipid interactions in model and biological membrane systems, in: E.N. Martonosi (Ed.), Membranes and Transport, vol. 1, Plenum, New York, 1982, pp. 115–123.
[9] M. Bloom, I.C.P. Smith, Manifestations of lipid–protein interactions in deuterium NMR, in: A. Watts, J.J.H.H.M. de Pont (Eds.), Progress in Protein–Lipid Interactions, vol. 1, Elsevier, Amsterdam, 1985, pp. 61–88.
[10] O.G. Mouritsen, M. Bloom, Mattress model of lipid–protein interactions in membranes, Biophys. J. 46 (1984) 141–153.
[11] A. Bienvenue, M. Bloom, J.H. Davis, P.F. Devaux, Evidence for protein-associated lipids from deuterium nuclear magnetic resonance studies of rhodopsin-dimyristoylphosphatidylcholine recombinants, J. Biol. Chem. 257 (1982) 3032–3038.
[12] A. Harrenga, H. Michel, The cytochrome *c* oxidase from *Paracoccus denitrificans* does not change the metal center ligation upon reduction, J. Biol. Chem. 274 (1999) 33296–33299.
[13] M. Svensson-Ek, J. Abramson, G. Larsson, S. Törnroth, P. Brzezinski, S. Iwata, The X-ray crystal structures of wild-type and EQ(I-286) mutant cytochrome *c* oxidases from *Rhodobacter sphaeroides*, J. Mol. Biol. 321 (2002) 329–339.
[14] T. Tsukihara, K. Shimokata, Y. Katayama, H. Shimada, K. Muramoto, H. Aoyama, M. Mochizuki, K. Shinzawa-Itoh, A. Yamashita, M. Yao, Y. Ishimura, S. Yoshikawa, The low-spin heme of cytochrome *c* oxidase as the driving element of the proton-pumping process, Proc. Natl. Acad. Sci. U. S. A. 100 (2003) 15304–15309.
[15] C. Lange, J.H. Nett, B.L. Trumpower, C. Hunte, Specific roles of protein–phospholipid interactions in the yeast cytochrome bc_1 complex structure, EMBO J. 20 (2001) 6591–6600.
[16] Z. Zhang, L. Huang, V.M. Shulmeister, Y.-I. Chi, K.K. Kim, L.-W. Hung, A.R. Crofts, E.A. Berry, S.-H. Kim, Electron transfer by domain movement in cytochrome bc_1, Nature 392 (1998) 677–684.
[17] E. Pebay-Peyroula, C. Dahout-Gonzalez, R. Kahn, V. Trézéguet, G.J.M. Lauquin, G. Brandolin, Structure of mitochondrial ADP/ATP carrier in complex with carboxyatractyloside, Nature 426 (2003) 39–44.
[18] A. Camara-Artigas, D. Brune, J.P. Allen, Interactions between lipids and bacterial reaction centers determined by protein crystallography, Proc. Natl. Acad. Sci. U. S. A. 99 (2002) 11055–11060.
[19] K.E. McAuley, P.K. Fyfe, J.P. Ridge, N.W. Isaacs, R.J. Cogdell, M.R. Jones, Structural details of an interaction between cardiolipin

and an integral membrane protein, Proc. Natl. Acad. Sci. U. S. A. 96 (1999) 14706–14711.
[20] P.K. Fyfe, J.P. Ridge, K.E. McAuley, R.J. Cogdell, N.W. Isaacs, M.R. Jones, Structural consequences of the replacement of glycine M203 with aspartic acid in the reaction center from *Rhodobacter sphaeroides*, Biochemistry 39 (2000) 5953–5960.
[21] T. Nogi, I. Fathir, M. Kobayashi, T. Nozawa, K. Miki, Crystal structures of photosynthetic reaction center and high-potential iron–sulfur protein from *Thermochromatium tepidum*: thermostability and electron transfer, Proc. Natl. Acad. Sci. U. S. A. 97 (2000) 13561–13566.
[22] P. Jordan, P. Fromme, H.T. Witt, O. Klukas, W. Saenger, N. Krauß, Three-dimensional structure of cyanobacterial photosystem I at 2.5 Å resolution, Nature 411 (2001) 909–917.
[23] G. Kurisu, H. Zhang, J.L. Smith, W.A. Cramer, Structure of the cytochrome b_6f complex of oxygenic photosynthesis: tuning the cavity, Science 302 (2003) 1009–1014.
[24] M. Jormakka, S. Tornroth, B. Byrne, S. Iwata, Molecular basis of proton motive force generation: structure of formate dehydrogenase-*N*, Science 295 (2002) 1863–1868.
[25] V. Yankovskaya, R. Horsefield, S. Törnröth, C. Luna-Chavez, H. Miyoshi, C. Léger, B. Byrne, G. Cecchini, S. Iwata, Architecture of succinate dehydrogenase and reactive oxygen species generation, Science 299 (2003) 700–704.
[26] F.I. Valiyaveetil, Y.F. Zhou, R. MacKinnon, Lipids in the structure, folding, and function of the KcsA K^+ channel, Biochemistry 41 (2002) 10771–10777.
[27] L.-O. Essen, R. Siegert, W.D. Lehmann, D. Oesterhelt, Lipid patches in membrane protein oligomers: crystal structure of the bacteriorhodopsin–lipid complex, Proc. Natl. Acad. Sci. U. S. A. 95 (1998) 11673–11678.
[28] H. Luecke, B. Schobert, H.-T. Richter, J.-P. Cartailler, J.K. Lanyi, Structure of bacteriorhodopsin at 1.55 Å resolution, J. Mol. Biol. 291 (1999) 899–911.
[29] H. Belrhali, P. Nollert, A. Royant, C. Menzel, J.P. Rosenbusch, E.M. Landau, E. Pebay-Peyroula, Protein, lipid and water organization in bacteriorhodopsin crystals: a molecular view of the purple membrane at 1.9 Å resolution, Structure 7 (1999) 909–917.
[30] K. Takeda, Y. Matsui, H. Sato, T. Hino, E. Kanamori, H. Okumura, T. Yamane, N. Kamiya, T. Kouyama, Deposition 1QM8 in the Protein Database. (2000).
[31] A.D. Ferguson, W. Welte, E. Hofmann, B. Lindner, O. Holst, J.W. Coulton, K. Diederichs, A conserved structural motif for lipopolysaccharide recognition by procaryotic and eucaryotic proteins, Struct. Fold. Des. 8 (2000) 585–592.
[32] P.F. Knowles, A. Watts, D. Marsh, Spin label studies of lipid immobilization in dimyristoylphosphatidylcholine-substituted cytochrome oxidase, Biochemistry 18 (1979) 4480–4487.
[33] J.F. Ellena, M.A. Blazing, M.G. McNamee, Lipid–protein interactions in reconstituted membranes containing acetylcholine receptor, Biochemistry 22 (1983) 5523–5535.
[34] J.R. Silvius, D.A. McMillen, N.D. Saley, P.C. Jost, O.H. Griffith, Competition between cholesterol and phosphatidylcholine for the hydrophobic surface of sarcoplasmic reticulum Ca^{2+}-ATPase, Biochemistry 23 (1984) 538–547.
[35] P.J. Brophy, L.I. Horváth, D. Marsh, Stoichiometry and specificity of lipid–protein interaction with myelin proteolipid protein studied by spin-label electron spin resonance, Biochemistry 23 (1984) 860–865.
[36] N.J.P. Ryba, L.I. Horváth, A. Watts, D. Marsh, Molecular exchange at the lipid–rhodopsin interface: spin-label electron spin resonance studies of rhodopsin–dimyristoyl phosphatidylcholine recombinants, Biochemistry 26 (1987) 3234–3240.
[37] L.I. Horváth, M. Drees, K. Beyer, M. Klingenberg, D. Marsh, Lipid–protein interactions in ADP–ATP carrier/egg phosphatidylcholine recombinants studied by spin-label ESR spectroscopy, Biochemistry 29 (1990) 10664–10669.
[38] S.J.C.J. Peelen, J.C. Sanders, M.A. Hemminga, D. Marsh, Stoichiometry, selectivity, and exchange dynamics of lipid–protein interaction with bacteriophage M13 coat protein studied by spin label electron spin resonance. Effects of protein secondary structure, Biochemistry 31 (1992) 2670–2677.
[39] L.I. Horváth, T. Heimburg, P. Kovachev, J.B.C. Findlay, K. Hideg, D. Marsh, Integration of a K^+ channel-associated peptide in a lipid bilayer: conformation, lipid–protein interactions, and rotational diffusion, Biochemistry 34 (1995) 3893–3898.
[40] R.L. Cornea, L.R. Jones, J.M. Autry, D.D. Thomas, Mutation and phosphorylation change the oligomeric structure of phospholamban in lipid bilayers, Biochemistry 36 (1997) 2960–2967.
[41] D. Marsh, Stoichiometry of lipid–protein interaction and integral membrane protein structure, Eur. Biophys. J. 26 (1997) 203–208.
[42] T. Páli, D. Bashtovyy, D. Marsh, Stoichiometry of lipid interaction with transmembrane proteins, deduced from the 3-D structures, to be published (2004).
[43] T. Okada, Y. Fujiyoshi, M. Silow, J. Navarro, E.M. Landau, Y. Shichida, Functional role of internal water molecules in rhodopsin revealed by X-ray crystallography, Proc. Natl. Acad. Sci. U. S. A. 99 (2002) 5982–5987.
[44] M.C. Surles, J.S. Richardson, D.C. Richardson, F.P. Brooks Jr., Sculpting protein interactively: continual energy minimization embedded in a graphical modeling system, Protein Sci. 3 (1994) 198–210.
[45] N.L. Allinger, Y.H. Yuh, J.-H. Lii, Molecular mechanics. The MM3 force field for hydrocarbons. 1, J. Am. Chem. Soc. 111 (1989) 8551–8566.
[46] D. Bashtovyy, D. Marsh, M.A. Hemminga, T. Páli, Molecular modelling studies on the spin-labelled major coat protein of the M13 bacteriophage in a phospholipid bilayer, Protein Sci. 10 (2001) 979–987.
[47] A. Watts, I.D. Volotovski, D. Marsh, Rhodopsin–lipid associations in bovine rod outer segment membranes. Identification of immobilized lipid by spin labels, Biochemistry 18 (1979) 5006–5013.
[48] R.D. Pates, A. Watts, R. Uhl, D. Marsh, Lipid–protein interactions in frog rod outer segment disc membranes. Characterization by spin labels, Biochim. Biophys. Acta 814 (1985) 389–397.
[49] N. Unwin, Nicotinic acetylcholine receptor at 9 Å resolution, J. Mol. Biol. 229 (1993) 1101–1124.
[50] A.C. Wallace, R.A. Laskowski, J.M. Thornton, LIGPLOT—a program to generate schematic diagrams of protein ligand interactions, Protein Eng. 8 (1995) 127–134.
[51] I. Pascher, M. Lundmark, P.-G. Nyholm, S. Sundell, Crystal structures of membrane lipids, Biochim. Biophys. Acta 1113 (1992) 339–373.
[52] D. Marsh, Lipid-binding proteins: structure of the phospholipid ligands, Protein Sci. 12 (2003) 2109–2117.
[53] I. Pascher, S. Sundell, K. Harlos, H. Eibl, Conformation and packing properties of membrane lipids: the crystal structure of sodium dimyristoylphosphatidylglycerol, Biochim. Biophys. Acta 896 (1987) 77–88.
[54] D. Marsh, T. Páli, Conformation and chain order of lipids in crystals of transmembrane proteins, to be published (2004).
[55] I. Pascher, The different conformations of the glycerol region of crystalline acylglycerols, Curr. Opin. Struct. Biol. 6 (1996) 439–448.
[56] J. Seelig, H.U. Gally, Investigation of phosphatidylethanolamine bilayers by deuterium and phosphorus-31 nuclear magnetic resonance, Biochemistry 15 (1976) 5199–5204.
[57] J. Seelig, H.U. Gally, R. Wohlgemuth, Orientation and flexibility of the choline head group in phosphatidylcholine bilayers, Biochim. Biophys. Acta 467 (1977) 109–119.
[58] A. Abe, J.E. Mark, Conformational energies and the random-coil dimensions and dipole-moments of the polyoxides $CH_3O[(CH_2)_yO]_xCH_3$, J. Am. Chem. Soc. 98 (1976) 6468–6476.
[59] P.J. Flory, Statistical Mechanics of Chain Molecules, Wiley, London, 1969.

[60] G.J. Kleywegt, K. Henrick, E.J. Dodson, D.M.F. van Aalten, Pound-wise but penny-foolish: how well do micromolecules fare in macromolecular refinement? Structure 11 (2003) 1051–1059.
[61] G. Cevc, D. Marsh, Phospholipid Bilayers. Physical Principles and Models, Wiley-Interscience, New York, 1987.
[62] D. Marsh, Lipid interactions with transmembrane proteins, Cell. Mol. Life Sci. 60 (2003) 1575–1580.
[63] T. Róg, M. Pasenkiewicz-Gierula, Cholesterol effects on the phosphatidylcholine bilayer nonpolar region: a molecular simulation study, Biophys. J. 81 (2001) 2190–2202.
[64] M. Kates, C.N. Joo, B. Palameta, T. Shier, Absolute stereochemical configuration of phytanyl (dihydrophytyl) groups in lipids of *Halobacterium cutirubrum*, Biochemistry 6 (1967) 3329–3338.
[65] M. Moser, D. Marsh, P. Meier, K.-H. Wassmer, G. Kothe, Chain configuration and flexibility gradient in phospholipid membranes. Comparison between spin-label electron spin resonance and deuteron nuclear magnetic resonance, and identification of new conformations, Biophys. J. 55 (1989) 111–123.
[66] H.U. Gally, W. Niederberger, J. Seelig, Conformation and motion of the choline head group in bilayers of dipalmitoyl-3-*sn*-phosphatidylcholine, Biochemistry 14 (1975) 3647–3652.
[67] A. Seelig, J. Seelig, Dynamic structure of fatty acyl chains in a phospholipid bilayer measured by deuterium magnetic resonance, Biochemistry 13 (1974) 4839–4845.
[68] V.E. Ahn, K.F. Faull, J.P. Whitelegge, A.L. Fluharty, G.G. Prive, Crystal structures of saposin B reveals a dimeric shell for lipid binding, Proc. Natl. Acad. Sci. U. S. A. 100 (2003) 38–43.
[69] H. Heller, M. Schaeffer, K. Schulten, Molecular dynamics simulation of a bilayer of 200 lipids in the gel and in the liquid-crystal phases, J. Phys. Chem. 97 (1993) 8343–8360.
[70] H. Heller, http://www.lrz-muenchen.de/~heller/membrane/membrane.html (2004).
[71] I. Therien, R. Moreau, P. Manjunath, Major proteins of bovine seminal plasma and high-density lipoprotein induce cholesterol efflux from epididymal sperm, Biol. Reprod. 59 (1998) 768–776.
[72] R. Moreau, P. Manjunath, Characterization of lipid efflux particles generated by seminal phospholipid-binding proteins, Biochim. Biophys. Acta 1438 (1999) 175–184.
[73] S.H. White, W.C. Wimley, Membrane protein folding and stability: physical principles, Annu. Rev. Biophys. Biomol. Struct. 28 (1999) 319–365.
[74] D.A. Wah, C. Fernández-Tornero, L. Sanz, A. Romero, J.J. Calvete, Sperm coating mechanism from the 1.8 Å crystal structure of PDC-109 phosphorylcholine complex, Structure 10 (2002) 505–514.
[75] L. Desnoyers, P. Manjunath, Major proteins of bovine seminal plasma exhibit novel interactions with phospholipid, J. Biol. Chem. 267 (1992) 10149–10155.
[76] M. Ramakrishnan, V. Anbazhagan, T.V. Pratap, D. Marsh, M.J. Swamy, Membrane insertion and lipid–protein interactions of bovine seminal plasma protein PDC-109 investigated by spin-label electron spin resonance spectroscopy, Biophys. J. 81 (2001) 2215–2225.
[77] A. Greube, K. Müller, E. Töpfer-Petersen, A. Herrmann, P. Müller, Influence of bovine seminal plasma protein PDC-109 on the physical state of membranes, Biochemistry 40 (2001) 8326–8334.
[78] M.J. Swamy, D. Marsh, V. Anbazhagan, M. Ramakrishnan, Effect of cholesterol on the interaction of seminal plasma protein, PDC-109 with phosphatidylcholine membranes, FEBS Lett. 528 (2002) 230–234.
[79] P. Müller, K.-R. Erlemann, K. Müller, J.J. Calvete, E. Töpfer-Petersen, K. Marienfeld, A. Herrmann, Biophysical characterization of the interaction of bovine seminal plasma protein PDC-109 with phospholipid vesicles, Eur. Biophys. J. 27 (1998) 33–41.
[80] M. Gasset, L. Magdaleno, J.J. Calvete, Biophysical study of the perturbation of model membrane structure caused by seminal plasma protein PDC-109, Arch. Biochem. Biophys. 374 (2000) 241–247.
[81] P. Müller, A. Greube, E. Töpfer-Petersen, A. Herrmann, Influence of the bovine seminal plasma protein PDC-109 on cholesterol in the presence of phospholipids, Eur. Biophys. J. 31 (2002) 438–447.
[82] T.J. Andreasen, M.G. McNamee, Inhibition of ion permeability control properties of acetylcholine receptor from Torpedo californica by long-chain fatty acids, Biochemistry 19 (1980) 4719–4726.
[83] T. Heidmann, R.E. Oswald, J.-P. Changeux, Multiple sites of action for noncompetitive blockers of acetylcholine receptor rich membrane fragments from *Torpedo marmorata*, Biochemistry 22 (1983) 3112–3127.
[84] D. Marsh, F.J. Barrantes, Immobilized lipid in acetylcholine receptor-rich membranes from *Torpedo marmorata*, Proc. Natl. Acad. Sci. U. S. A. 75 (1978) 4329–4333.
[85] D. Marsh, A. Watts, F.J. Barrantes, Phospholipid chain immobilization and steroid rotational immobilization in acetylcholine receptor-rich membranes from *Torpedo marmorata*, Biochim. Biophys. Acta 645 (1981) 97–101.
[86] S. Mantripragada, L.I. Horváth, H.R. Arias, G. Schwarzmann, K. Sandhoff, F.J. Barrantes, D. Marsh, Lipid–protein interactions and effect of local anesthetics in acetylcholine receptor-rich membranes from *Torpedo marmorata* electric organ, Biochemistry 42 (2003) 9167–9175.
[87] A. Miyazawa, Y. Fujiyoshi, N. Unwin, Structure and gating mechanism of the acetylcholine receptor pore, Nature 423 (2003) 949–955.
[88] M. Criado, H. Eibl, F.J. Barrantes, Functional properties of the acetylcholine receptor incorporated in model lipid membranes, J. Biol. Chem. 259 (1984) 9188–9198.
[89] C. Sunshine, M.G. McNamee, Lipid modulation of nicotinic acetylcholine receptor function—the role of neutral and negatively charged lipids, Biochim. Biophys. Acta 1108 (1992) 240–246.
[90] H.H. Wang, J.Z. Yeh, T. Narahashi, Interaction of spin-labelled local anesthetics with the sodium channel of squid axon membranes, J. Membr. Biol. 66 (1982) 227–233.
[91] J. Tigyi, K. Hideg, T. Lakatos, Study of nerve conduction with spin-labelled anesthetics, in: Yu. A. Ouchinnikov (Ed.), Progress in Bioorganic Chemistry and Molecular Biology, Elsevier, Amsterdam, 1984, pp. 501–508.
[92] A. Brisson, P.F. Devaux, J.-P. Changeux, Effet anesthésique local de plusieurs composés liposolubles sur la réponse de l'électroplaque de gymnote à la carbamylcholine et sur la liaison de l'acétylcholine au récepteur cholinergique de torpille, C. R. Acad. Sci. Paris 280 D (1975) 2153–2156.
[93] L.I. Horváth, H.R. Arias, H.O. Hankovszky, K. Hideg, F.J. Barrantes, D. Marsh, Association of spin-labeled local anaesthetics at the hydrophobic surface of acetylcholine receptor in native membranes from *Torpedo marmorata*, Biochemistry 29 (1990) 8707–8713.
[94] B. Hille, pH-dependent rate of action of local anesthetics on node of ranvier, J. Gen. Physiol. 69 (1977) 475–496.
[95] J. Miyazaki, K. Hideg, D. Marsh, Interfacial ionization and partitioning of membrane-bound local anaesthetics, Biochim. Biophys. Acta 1103 (1992) 62–68.
[96] O.T. Jones, M.G. McNamee, Annular and nonannular binding sites for cholesterol associated with the nicotinic acetylcholine receptor, Biochemistry 27 (1988) 2364–2374.
[97] S. Lamberth, H. Schmid, M. Muenchbach, T. Vorherr, J. Krebs, E. Carafoli, C. Griesinger, NMR solution structure of phospholamban, Helv. Chim. Acta 83 (2000) 2141–2152.
[98] Y. Kimura, K. Kurzydlowski, M. Tada, D.H. MacLennan, Phospholamban inhibitory function is activated by depolymerization, J. Biol. Chem. 272 (1997) 15061–15064.
[99] L.G. Reddy, J.M. Autry, L.R. Jones, D.D. Thomas, Co-reconstruction of phospholamban mutants with the Ca-ATPase reveals dependence of inhibitory function on phospholamban structure, J. Biol. Chem. 274 (1999) 7649–7655.

[100] J. Fuji, K. Maruyama, M. Tada, D.H. MacLennan, Expression and site-specific mutagenesis of phospholamban: studies of residues involved in phosphorylation and pentamer formation., J. Biol. Chem. 264 (1989) 12950–12955.
[101] C.B. Karim, C.G. Marquardt, J.D. Stamm, G. Barany, D.D. Thomas, Synthetic null-cysteine phospholamban analogue and the corresponding transmembrane domain inhibit the Ca-ATPase, Biochemistry 39 (2000) 10892–10897.
[102] A. Arora, I.M. Williamson, A.G. Lee, D. Marsh, Lipid–protein interactions with cardiac phospholamban studied by spin-label electron spin resonance, Biochemistry 42 (2003) 5151–5158.
[103] M.R.R. de Planque, D.V. Greathouse, R.E. Koeppe II, H. Schäfer, D. Marsh, J.A. Killian, Influence of lipid/peptide hydrophobic mismatch on the thickness of diacylphosphatidylcholine bilayers. A ^{2}H NMR and ESR study using designed transmembrane α-helical peptides and gramicidin A, Biochemistry 37 (1998) 9333–9345.
[104] M.R.R. de Planque, J.A.W. Kruijtzer, R.M.J. Liskamp, D. Marsh, D.V. Greathouse, R.E. Koeppe II, B. De Kruijff, J.A. Killian, Different membrane anchoring positions of tryptophan and lysine in synthetic transmembrane α-helical peptides, J. Biol. Chem. 274 (1999) 20839–20846.
[105] J. Pérez-Gil, C. Casals, D. Marsh, Interactions of hydrophobic lung surfactant proteins SP-B and SP-C with dipalmitoylphosphatidylcholine and dipalmitoylphosphatidylglycerol bilayers studied by electron spin resonance spectroscopy, Biochemistry 34 (1995) 3964–3971.
[106] N.M. Green, Avidin, Adv. Protein Chem. 29 (1975) 85–133.
[107] M.J. Swamy, D. Marsh, Specific surface association of avidin with *N*-biotinylphosphatidylethanolamine membrane assemblies: effect on lipid phase behavior and acyl-chain dynamics, Biochemistry 40 (2001) 14869–14877.
[108] D.L. Scott, S.P. White, Z. Otwinowski, W. Yuan, M.H. Gelb, P.B. Sigler, Interfacial catalysis: the mechanism of phospholipase A_2, Science 250 (1990) 1541–1546.
[109] M.J. Swamy, D. Marsh, Spin-label studies on the anchoring and lipid–protein interactions of avidin with *N*-biotinylphosphatidylethanolamines in lipid bilayer membranes, Biochemistry 36 (1997) 7403–7407.
[110] P.C. Weber, D.H. Ohlendorf, J.J. Wendoloski, F.R. Salemme, Structural origins of high-affinity biotin binding to streptavidin, Science 243 (1989) 85–88.
[111] S.A. Darst, M. Ahlers, P.H. Meller, E.W. Kubalek, R. Blankenburg, H.O. Ribi, H. Ringsdorf, R.D. Kornberg, Two-dimensional crystals of streptavidin on biotinylated lipid layers and their interactions with biotinylated macromolecules, Biophys. J. 59 (1991) 387–396.
[112] A. Arora, D. Marsh, Protein-induced vertical lipid dislocation in a model membrane system: spin-label relaxation studies on avidin-biotinylphosphatidylethanolamine interactions, Biophys. J. 75 (1998) 2915–2922.
[113] M.B. Sankaram, D. Marsh, Protein–lipid interactions with peripheral membrane proteins, in: A. Watts (Ed.), New Comprehensive Biochemistry, Protein–Lipid Interactions, vol. 25, Elsevier, Amsterdam, 1993, pp. 127–162.
[114] D. Marsh, Specificity of lipid–protein interactions, in: A.G. Lee (Ed.), Biomembranes, vol. 1, JAI Press, Greenwich, CT, 1995, pp. 137–186.
[115] P.F. Knowles, A. Watts, D. Marsh, Spin label studies of headgroup specificity in the interaction of phospholipids with yeast cytochrome oxidase, Biochemistry 20 (1981) 5888–5894.
[116] G.L. Powell, P.F. Knowles, D. Marsh, Association of spin-labelled cardiolipin with dimyristoylphosphatidylcholine-substituted bovine heart cytochrome *c* oxidase. A generalized specificity increase rather than highly specific binding sites, Biochim. Biophys. Acta 816 (1985) 191–194.
[117] H. Görrissen, D. Marsh, A. Rietveld, B. De Kruijff, Apocytochrome *c* binding to negatively charged lipid dispersions studied by spin-label electron spin resonance, Biochemistry 25 (1986) 2904–2910.
[118] A. Kostrzewa, T. Páli, W. Froncisz, D. Marsh, Membrane location of spin-labelled cytochrome *c* determined by paramagnetic relaxation agents, Biochemistry 39 (2000) 6066–6074.
[119] J.H. Kleinschmidt, G.L. Powell, D. Marsh, Cytochrome *c*-induced increase of motionally restricted lipid in reconstituted cytochrome *c* oxidase membranes, revealed by spin-label ESR spectroscopy, Biochemistry 37 (1998) 11579–11585.
[120] T. Tsukihara, H. Aoyama, E. Yamashita, T. Tomizaki, H. Yamaguchi, K. Shinzawa-Itoh, R. Nakashima, R. Yaono, S. Yoshikawa, The whole structure of the 13-subunit oxidized cytochrome *c* oxidase at 2.8 Å, Science 272 (1996) 1136–1144.
[121] L. Banci, I. Bertini, H.B. Gray, C. Luchinat, T. Reddig, A. Rosato, P. Turano, Solution structure of oxidized horse heart cytochrome *c*, Biochemistry 36 (1997) 9867–9877.
[122] J.E. Mahaney, J. Kleinschmidt, D. Marsh, D.D. Thomas, Effects of melittin on lipid–protein interactions in sarcoplasmic reticulum membranes, Biophys. J. 63 (1992) 1513–1522.
[123] T. Weimbs, W. Stoffel, Proteolipid protein (PLP) of CNS myelin: positions of free, disulfide-bonded, and fatty acid thioester-linked cysteine residues and implications for the membrane topology of PLP, Biochemistry 31 (1992) 12289–12296.
[124] W.A. Surewicz, M.A. Moscarello, H.H. Mantsch, Fourier transform infrared spectroscopic investigation of the interaction between myelin basic protein and dimyristoyl phosphatidylglycerol bilayers, Biochemistry 26 (1987) 3881–3886.
[125] M.B. Sankaram, P.J. Brophy, D. Marsh, Lipid–protein and protein–protein interactions in double recombinants of myelin proteolipid apoprotein and myelin basic protein with dimyristoylphosphatidylglycerol, Biochemistry 30 (1991) 5866–5873.
[126] M.B. Sankaram, P.J. Brophy, D. Marsh, Spin label ESR studies on the interaction of bovine spinal cord myelin basic protein with dimyristoylphosphatidylglycerol dispersions, Biochemistry 28 (1989) 9685–9691.
[127] M.J. Swamy, L.I. Horváth, P.J. Brophy, D. Marsh, Interactions between lipid-anchored and transmembrane proteins. Spin-label ESR studies on avidin-biotinyl phosphatidylethanolamine in membrane recombinants with myelin proteolipid protein, Biochemistry 38 (1999) 16333–16339.
[128] W.A. Hendrickson, A. Pahler, J.L. Smith, Y. Satow, E.A. Merritt, R.P. Phizackerley, Crystal-structure of core streptavidin determined from multiwavelength anomalous diffraction of synchrotron radiation, Proc. Natl. Acad. Sci. U. S. A. 86 (1989) 2190–2194.
[129] R. Schroeder, E. London, D. Brown, Interactions between saturated acyl chains confer detergent resistance on lipids and glycosylphosphatidylinositol (GPI)-anchored proteins: GPI-anchored proteins in liposomes and cells show similar behavior, Proc. Natl. Acad. Sci. U. S. A. 91 (1994) 12130–12134.
[130] K. Simons, E. Ikonen, Functional rafts in cell membranes, Nature 387 (1997) 569–572.